BAF subunit switching regulates chromatin accessibility to control cell cycle exit in the developing mammalian cortex

Simon M.G. Braun,[1,2,3,4,9] Ralitsa Petrova,[5,6,7,9] Jiong Tang,[1,2,3,8] Andrey Krokhotin,[1,2,3] Erik L. Miller,[1,2,3] Yitai Tang,[3] Georgia Panagiotakos,[5,6,7] and Gerald R. Crabtree[1,2,3]

[1]Howard Hughes Medical Institute, Stanford University, Stanford, California 94305, USA; [2]Department of Developmental Biology, Stanford University, California 94305, USA; [3]Department of Pathology, Stanford University, California 94305, USA; [4]Department of Genetic Medicine and Development, Faculty of Medicine, University of Geneva, 1211 Geneva, Switzerland; [5]Department of Biochemistry and Biophysics, University of California at San Francisco, San Francisco, California 94143, USA; [6]Eli and Edythe Broad Center of Regeneration Medicine and Stem Cell Research, University of California at San Francisco, San Francisco, California 94143, USA; [7]Kavli Institute for Fundamental Neuroscience, University of California at San Francisco, San Francisco, California 94143, USA; [8]Singapore Bioimaging Consortium, Agency for Science Technology and Research (A*STAR), Singapore 138667, Singapore

mSWI/SNF or BAF chromatin regulatory complexes are dosage-sensitive regulators of human neural development frequently mutated in autism spectrum disorders and intellectual disability. Cell cycle exit and differentiation of neural stem/progenitor cells is accompanied by BAF subunit switching to generate neuron-specific nBAF complexes. We manipulated the timing of BAF subunit exchange in vivo and found that early loss of the npBAF subunit BAF53a stalls the cell cycle to disrupt neurogenesis. Loss of BAF53a results in decreased chromatin accessibility at specific neural transcription factor binding sites, including the pioneer factors SOX2 and ASCL1, due to Polycomb accumulation. This results in repression of cell cycle genes, thereby blocking cell cycle progression and differentiation. Cell cycle block upon *Baf53a* deletion could be rescued by premature expression of the nBAF subunit BAF53b but not by other major drivers of proliferation or differentiation. WNT, EGF, bFGF, SOX2, c-MYC, or PAX6 all fail to maintain proliferation in the absence of BAF53a, highlighting a novel mechanism underlying neural progenitor cell cycle exit in the continued presence of extrinsic proliferative cues.

[*Keywords*: BAF complex; cell cycle exit; cell type-specific transcriptional networks; chromatin accessibility; cortical development; neurogenesis]

Supplemental material is available for this article.

Received July 8, 2020; revised version accepted January 8, 2021.

Neurogenesis in vertebrates is accompanied by dramatic alterations in chromatin structure correlating with temporally precise developmental transitions. Many human neurologic diseases have their origin in mutations in chromatin regulators, calling attention to the different roles played by these chromatin regulatory mechanisms (Santen et al. 2012). One event that correlates with cell cycle exit in the mammalian nervous system is a switch in subunit composition of BAF or mSWI/SNF complexes (Ho and Crabtree 2010). These ATP-dependent chromatin regulators are similar to yeast SWI/SNF and *Drosophila* BAP complexes, and in mammals are comprised of 15 subunits that are combinatorially assembled to produce several hundred complexes (Wang et al. 1996a,b; Olave et al. 2002; Lessard et al. 2007; Wu et al. 2007; Yoo et al. 2009; Ninkovic et al. 2013). BAF subunits are exchanged at the transitions from pluripotent stem cells to neural stem/progenitor cells (NSPCs) to neurons. As NSPCs in the developing nervous system exit the cell cycle, neural progenitor BAF (npBAF) complexes containing BAF53a (*Actl6a*), BAF45a/d, and SS18 switch subunits to produce highly specific nBAF complexes containing subunits BAF53b (*Actl6b*), BAF45b/c, and CREST (Lessard et al.

[9]**These authors contributed equally to this work.**
Corresponding authors: georgia.panagiotakos@ucsf.edu, crabtree@stanford.edu
Article published online ahead of print. Article and publication date are online at http://www.genesdev.org/cgi/doi/10.1101/gad.342345.120.

2007). These complexes are highly stable in vitro, allowing for the generation of distinct composite surfaces, much like letters in words (Wu et al. 2009), thought to be responsible for their wide range of biologically specific activities (Hota and Bruneau 2016).

Consistent with diverse roles for these complexes during neural development, mutations in BAF subunits are frequently associated with neurodevelopmental diseases, including autism spectrum disorders (ASD), intellectual disability (ID), and speech disorders. Mutations in *SMARCB1* (encoding BAF47), *ARID1a/b* (encoding Baf250a/b), or *SMARCA4* (encoding Brg1/Brm) cause Coffin-Siris and Nicolaides-Baraitser syndromes (Santen et al. 2012, 2013; Tsurusaki et al. 2012, 2014; Van Houdt et al. 2012), while mutations in *ACTL6B* (encoding BAF53b) cause ASD (Bell et al. 2019; Wenderski et al. 2020). Recent studies have also found that monoallelic mutations of *ARID1B* are the most frequent cause of de novo intellectual disability (The Deciphering Developmental Disorders Study 2015), and GWAS studies have implicated sequence variation in *PBRM1* (encoding BAF180) in exceptional intellectual ability (Sniekers et al. 2017; Savage et al. 2018). The compromising mutations are typically heterozygous loss-of-function alleles, indicating a dosage-sensitive role for BAF subunits in fundamental aspects of human nervous system development.

Cell cycle exit in the developing brain is a highly orchestrated process that functions like an "AND" gate, integrating numerous pathways rather than operating under the control of a single master regulator. Intrinsic cues and extrinsic signals, including depolarization, voltage-gated channels, neurotransmitter receptors, mitotic spindle orientation, growth factor signaling pathways, cellular metabolism, and transcriptional mechanisms, contribute to cell cycle exit in NSPCs (Chenn and Walsh 2002; Dehay and Kennedy 2007; Kriegstein and Alvarez-Buylla 2009; Knobloch et al. 2013). It remains unclear, however, how these mechanisms are coordinated and synchronized with the onset of neural differentiation. While flies lack the subunit switch that characterizes mammalian neural development, in the *Drosophila* nervous system, the Osa subunit of the homologous BAP complex is necessary for progression of neural progenitors to control the number of transit-amplifying divisions (Eroglu et al. 2014). In mammals, exchange of BAF subunits at the transition from cycling NSPCs to postmitotic neurons is driven by *miR-9* and *miR-124*, which repress BAF53a. Extending expression of *Baf53a* by deleting the *miR-9/124* binding sites from its 3′ UTR results in excessive progenitor proliferation in the neural tube (Yoo et al. 2009). Moreover, executing this microRNA/chromatin switch to drive expression of nBAF subunits in human fibroblasts effectively converts these cells into neurons (Yoo et al. 2011; Victor et al. 2014). These findings are consistent with observations that BAF53b and CREST mutant mice have normal NSPC proliferation and instead display phenotypes associated with neuronal differentiation and maturation, including impaired dendritic morphogenesis and synaptic plasticity (Aizawa et al. 2004; Wu et al. 2007; Vogel-Ciernia et al. 2013). Nevertheless, while the npBAF to nBAF subunit exchange temporally corresponds to cell cycle exit, the role of suppression of npBAF subunits and replacement by nBAF subunits, and the mechanisms by which this switch is involved in cell cycle regulation, have not been explored.

Here, we investigated the role of BAF subunit switching in NSPC cell cycle exit in the embryonic mouse brain. We found that early removal of *Baf53a* using conditional deletion leads to loss of both BAF53a and β-actin from BAF complexes, resulting in blocked cell cycle progression, precocious NSPC cell cycle exit, and impaired cortical neurogenesis. We also found that BAF53a-containing npBAF complexes are required to promote chromatin accessibility at a broad array of cell cycle and NSPC identity genes through opposition of Polycomb repressive complexes. Importantly, we find that cell cycle block resulting from early *Baf53a* deletion can be rescued by expression of neuron-specific nBAF subunits, allowing for cell cycle exit and neuronal differentiation. Other major regulators of NSPC proliferation, including constitutively active WNT signaling, all fail to rescue *Baf53a* deletion-induced cell cycle block, indicating that BAF53a functions downstream from these regulators of proliferation. We propose that the switch from npBAF to nBAF chromatin regulators controls the timing of cell cycle exit in the developing cortex and provides a novel mechanism by which NSPC cell cycle exit occurs in the presence of continued stimulation by extrinsic factors.

Results

BAF53a regulates cell cycle progression in the developing cortex

During brain development, NSPC cell cycle exit and the subsequent onset of neuronal differentiation are correlated with repression of BAF53a and activation of BAF53b. Consistent with this, we observed that BAF53a is enriched in SOX2-expressing radial glia and TBR2-expressing intermediate progenitor cells (IPCs) in the ventricular and subventricular zones of the mouse embryonic cortex (VZ and SVZ, respectively). In contrast, BAF53b is highly expressed in MAP2ab+ neurons in the cortical plate (CP) (Fig. 1A). Similarly, analysis of published single cell RNA-seq data (Telley et al. 2019) from the developing mouse cortex at embryonic day 12 (E12) to E15 confirmed that npBAF subunit expression (*Baf53a*, *Baf45d*, and *Ss18*) is enriched in NSPCs in the VZ and SVZ, and nBAF subunits (*Baf53b*, *Baf45b*, and *Crest*) are expressed in cortical neurons, with a brief period of overlap between *Baf53a* and *Baf53b* transcript expression at intermediate stages of NPC differentiation and lineage progression (Supplemental Fig. S1A).

To investigate whether BAF53a is required for cell cycle progression in the nervous system, we employed a conditional genetic approach to delete *Baf53a*. As constitutive deletion of *Baf53a* leads to early embryonic lethality (data not shown), we generated *Baf53a* conditional mutant mice in which exons 4 and 5 are flanked by loxP sites, *Baf53a*$^{fl/fl}$ (Supplemental Fig. S1C). *Baf53a*$^{fl/-}$ mice were

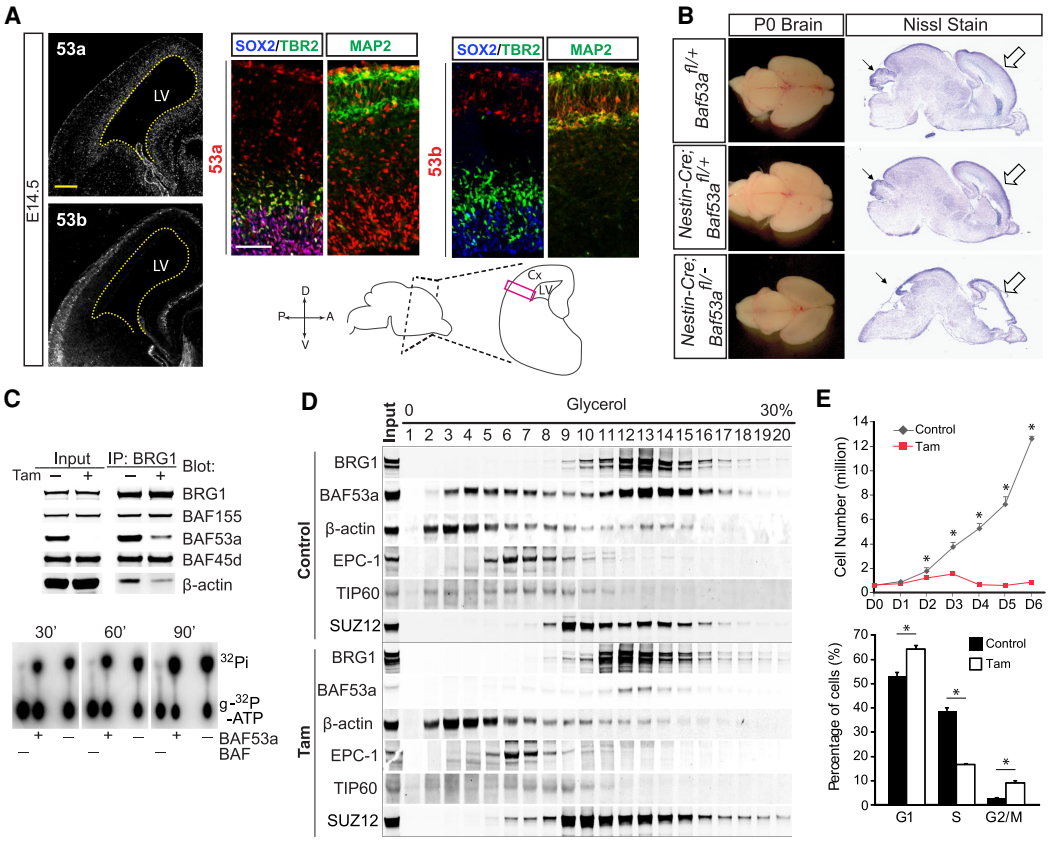

Figure 1. BAF53a regulates cell cycle progression in the developing cortex. (*A*) Representative coronal sections through the developing mouse brain at E14.5 depicting expression of BAF53a (*top left*) and BAF53b (*bottom left*). Dashed line delineates the wall of the lateral ventricle (LV). (*Middle*) Immunofluorescence staining shows BAF53A expression in SOX2+ (blue) and TBR2+ (green) neural stem and intermediate progenitor cells, respectively. (*Right*) Immunolabeling for BAF53b and MAP2 (green) reveals strong BAF53b expression in postmitotic neurons in the cortical plate at E14.5. Scale bars, 100 µm. Note: The BAF53a antibody cross-reacts with BAF53b in immunostainings of brain sections. (*B*) BAF53a mutant brains at P0. Photomicrographs of control, heterozygous, and BAF53a mutant brains at P0 (*left*) and Nissl stains of sagittal sections (*right*). Closed arrow points to cerebellum and open arrow indicates the neocortex. (*C*, *top* panel) Immunoprecipitation and western blot analysis of BAF proteins in control and *Baf53a* mutant nuclear extracts using an anti-BRG1 antibody. (*Bottom* panel) γ-^{32}P labeled-ATP was used as substrate to assess BAF ATPase activity, separated by chromatography and visualized by autoradiography. (*D*) Western blot on BAF53a-deficient and control nuclear glycerol gradient (0%–30%) fractions analyzed for BAF, PRC2, and TIP60 complex components. (*E*, *top* panel) Growth curve of *Actin-CreER*; *Baf53a*$^{fl/-}$ neurospheres for 6 d after tamoxifen (Tam) or ethanol (EtOH) control treatment. (*Bottom panel*) Quantification of cell cycle FACS analysis of *Actin-CreER*; *Baf53a*$^{fl/-}$ neurospheres. Cells were treated with BrdU 2 h before collection and harvested 72 h after tamoxifen administration for FACS. $n = 3$. Error bars represent SEM. (*) $P < 0.05$.

crossed with *Nestin-Cre* mice to inactivate *Baf53a* in NSPCs throughout the brain beginning at E10.5, before its normal developmental repression. *Nestin-Cre; Baf53a*$^{fl/-}$ (BAF53a mutant) mice survived to birth but died perinatally due to a failure to nurse. CRE-mediated deletion of *Baf53a* was very robust, as BAF53a levels were significantly reduced in BAF53a mutant forebrains by E14.5 (Supplemental Fig. S1B,G,H). The expression pattern of BAF53b was not significantly altered in BAF53a mutant mice (Supplemental Fig. S1D). BAF53a mutants were severely microcephalic with a dramatic reduction of cortical thickness, enlarged lateral ventricles, and a hypoplastic cerebellum (Fig. 1B; Supplemental Fig. S1E), suggesting a direct role for BAF53a in the control of brain size.

To assess BAF complex assembly and function biochemically, we bred conditional BAF53a mutant mice to transgenic mice expressing a tamoxifen-inducible form of CRE recombinase (CreER) (Brocard et al. 1997) under the control of the Actin promoter (*Actin-CreER;Baf53a*$^{fl/-}$). We then cultured E12.5 NSPCs isolated from *Actin-CreER;Baf53a*$^{fl/-}$ mice in vitro. Following tamoxifen treatment, multisubunit BAF complexes continued to assemble in mutant cells, as shown by immunoprecipitation for the core BAF complex subunit BRG1 and sucrose gradient sedimentation analysis (Fig. 1C,D). We found that complexes containing BRG1 and other npBAF subunits, but lacking BAF53a, lacked β-actin but maintained normal DNA-dependent ATPase activity (Fig. 1C,D; Supplemental Fig. S2A), suggesting that BAF53a and β-actin are not required for BAF complex assembly and function. Loss of these subunits also did not alter global chromatin affinity of the BAF complex in NSPCs (Supplemental Fig. S2B).

The proliferation of NSPCs lacking BAF53a, however, was severely impaired in culture, with mutant cells stalled at G1 and G2/M phases of the cell cycle (Fig. 1E). In support of a mechanism of cell cycle arrest, we found that deletion of *Baf53a* results in a significant increase in anaphase bridges (Supplemental Fig. S2C), a hallmark of improper segregation of daughter chromosomes during mitosis. Cells with anaphase bridges activate the decatenation checkpoint through the action of ATR/ATM kinases and undergo apoptosis (Downes et al. 1994). Consistent with decatenation checkpoint-induced cell death, we observed an increase in apoptosis in cultured NSPCs following *Baf53a* deletion (Supplemental Fig. S2D). Using a second, complementary strategy, we introduced lentiviruses expressing *miR-9* and *miR-124* into NSPCs in vitro. This induced a dramatic early reduction in BAF53a levels and produced a prominent G2/M cell cycle arrest similar to that seen in BAF53a mutant cells (Supplemental Fig. S2E,F). In line with these in vitro findings, following a 3-h pulse of the thymidine analog bromodeoxyuridine (BrdU) in vivo, we observed a near-complete absence of BrdU-labeled cells adjacent to the ventricles in BAF53a mutant mice, consistent with a failure of mutant NSPCs to progress to G2/M at E14.5 and E15.5 (Supplemental Fig. S1F–H). Together, these data suggest that early ablation of BAF53a results in defects in cell cycle progression and NSPC proliferation, in part due to the decatenation checkpoint.

Baf53a *deletion impairs the maintenance of NSPCs in the cortical germinal zones*

To characterize the consequences of early ablation of BAF53a on cortical neurogenesis, we performed immunofluorescence staining for the proliferation marker KI67 and the mitotic indicator phosphorylated histone H3 (PH3) (Fig. 2A,B; Supplemental Fig. 3A–C). PH3+ cells are normally found adjacent to the ventricular wall and scattered in the SVZ in control mice (Fig. 2B). In E15.5 BAF53a mutant mice, we observed an accumulation of large, round PH3+ and KI67+ cells in the VZ and SVZ, further highlighting a potential G2/M cell cycle block (Fig. 2A,B; Supplemental Fig. S3A–C). These abnormally large PH3+ cells persisted at later developmental stages (Supplemental Fig. S3C) and were accompanied by elevated cleaved caspase 3 staining, indicating increased cell death upon *Baf53a* deletion (Fig. 2A,B; Supplemental Fig. S3D) and consistent with cells failing the decatenation checkpoint. Strikingly, immunostaining for NSPC markers also revealed substantial disorganization of the germinal zones in BAF53a mutants. In control mice, PAX6 and TBR2 label discrete populations of VZ apical progenitors and SVZ IPCs, respectively. However, in BAF53a mutant mice, the NSPC pools appear mixed (Fig. 2C), with displacement of radial glial cells away from the ventricular wall and accumulation of TBR2+ IPCs closer to the ventricle. We also observed an increase in PAX6 and TBR2 coexpression, suggestive of abnormal mixing of cell identity markers in BAF53a knockout NSPC populations. Immunostaining for the radial glial cell marker phospho-Vimentin (pVIM) further illuminated a disruption of the neurogenic niche in BAF53a mutant mice (Fig. 2D), with increased pVIM+ cells, often coexpressing the IPC marker TBR2, localized in the SVZ away from the ventricle. In line with previous studies demonstrating that pVIM expression is largely restricted to mitotic radial glia (Kamei et al. 1998), colabeling for pVIM and the M-phase marker PH3 also revealed an almost complete overlap between these markers in *Baf53a* cKOs (Supplemental Fig. S3B), supporting the idea that a substantial fraction of radial glial cells are stalled at G2/M away from the ventricle in the SVZ. Importantly, in mutant brains, both pVIM+ radial glia and TBR2+ IPCs also expressed high levels of H2AX (Fig. 2D, insets), indicating an accumulation of DNA double-stranded breaks in both progenitor pools and consistent with the increased number of anaphase bridges we observed in vitro (Supplemental Fig. S2C). Collectively, these data provide additional support for the occurrence of checkpoint arrest in BAF53a mutant radial glia and IPCs.

The disorganization of the progenitor pools in BAF53a mutant mice was reflected in the CP, where newborn neuron populations were also disrupted. During normal neurogenesis, cortical layers are generated following successive rounds of progenitor divisions and the concomitant migration and differentiation of newborn neurons into the CP. Interestingly, we detected increased DCX-expressing neuroblasts in the VZ of BAF53a mutant mice, suggesting precocious differentiation in a small subset of mutant NSPCs (Fig. 2E). In E15.5 control mice, the CP was observed as a dense layer of NEUN+ neuronal cell bodies overlying the intermediate zone, whereas in mutant mice, the NEUN+ domain was expanded, and MAP2ab+ neuronal processes lost their vertical organization (Fig. 2E). Immunostaining for BLBP revealed irregular radial glial fibers in BAF53a mutant brains and a substantial accumulation of radial glial cell somata mislocalized abventricularly in the SVZ (Fig. 2E; Supplemental Fig. S6D), suggesting that altered migration secondary to disrupted radial glial fiber integrity may at least partially contribute to the observed changes in the distribution of postmitotic neurons in mutant mice. These apparent defects in differentiation were further amplified at later time points in cortical development. BrdU pulse-chase experiments revealed that the majority of NSPCs labeled at E15.5 failed to give rise to upper layer neurons that migrated into the CP by E18.5 (Supplemental Fig. S3E). Using immunostaining for various markers of laminar identity at E18.5, we also found that TBR1-, CTIP2-, and SATB2-expressing neurons were intermixed and failed to form distinct layers. CUX1-expressing upper layer neurons appeared to be drastically reduced (Fig. 2F), as were BRN1-expressing neurons (Supplemental Fig. S3F), suggesting a near-complete absence of later-generated neuronal cell types. These defects in upper-layer neurogenesis may be due to the timing of the *Nestin-Cre* deletion and the resulting loss of BAF53a protein, which may only be complete after deep layer neurons are already generated. Taken together, this phenotypic analysis reveals a central role for BAF53a in cortical neurogenesis. Early

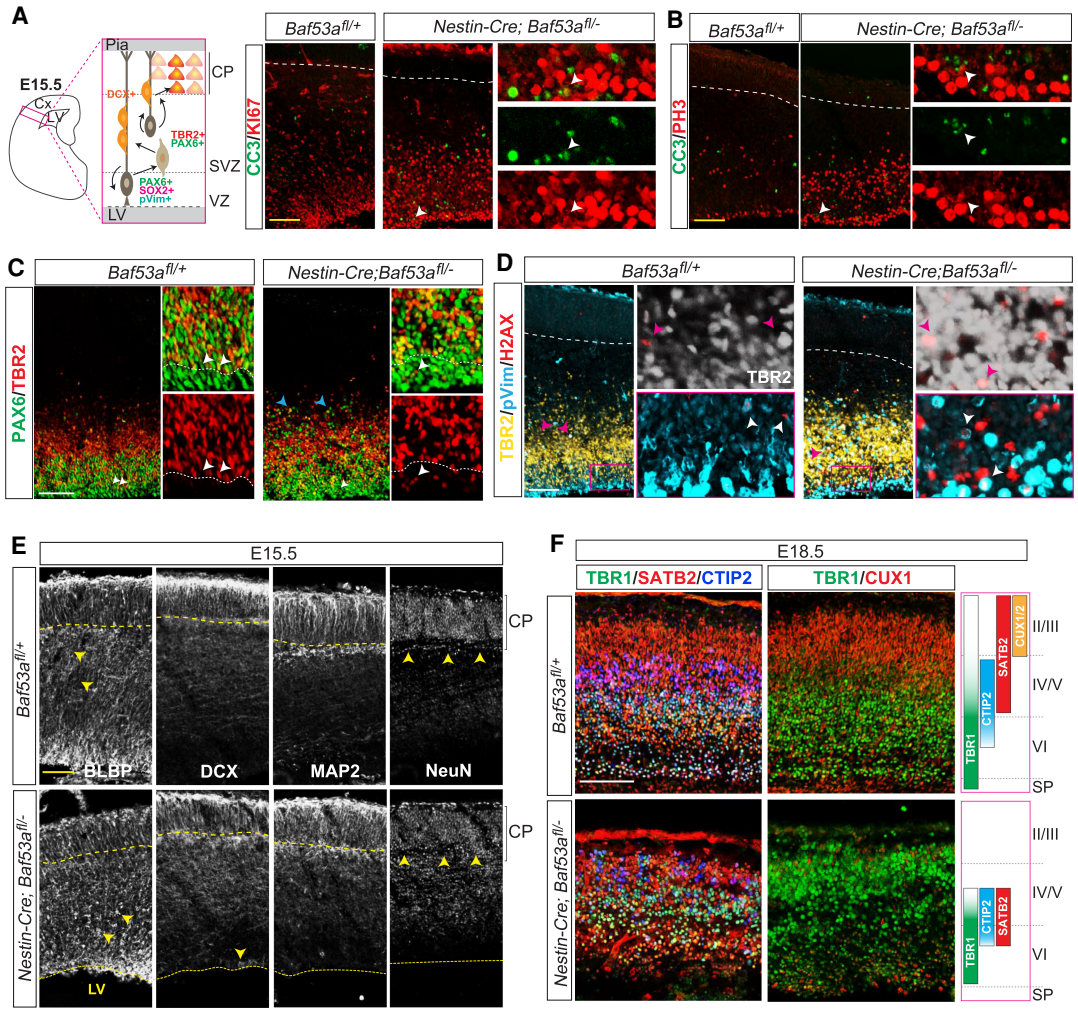

Figure 2. *Baf53a* deletion impairs the maintenance of neural stem and progenitor populations in the germinal zones of the cortex. (*A*,*B*, *left*) Schematic of mouse cortical neurogenesis depicting cortical radial glia (brown), and their progeny, newly generated (PAX6+TBR2+) and differentiating (PAX6−TBR2+) intermediate progenitor cells (tan) and migratory neuroblasts (orange), as well as cell type-specific markers expressed by each population. Immunostaining for the proliferation marker KI67 (*red*; *A*), or the M-phase marker phospho-histone H3 (PH3; red; *B*), showing colocalization with the cell apoptosis marker cleaved caspase 3 (CC3, green) in E15.5 BAF53a mutant cortex. Scale bar, 100 µm. (*C*) Colabeling for the radial glia and intermediate progenitor markers PAX6 (green) and TBR2 (red), respectively, depicts disorganization of the stem and progenitor pools in the ventricular and subventricular zones (VZ/SVZ; *insets*) in E15.5 BAF53a mutant brains. White arrowheads point to TBR2+ cells, highlighting the presence of IPCs in the VZ of mutant brains, and blue arrowheads point to PAX6+ cells further away from the ventricle in mutant mice compared with controls. Scale bar, 100 µm. (*D*) Immunostaining for the radial glia and intermediate progenitor markers phospho-Vimentin (pVIM, cyan) and TBR2 (amber or white), respectively, further highlights the disorganization of the VZ/SVZ in E15.5 BAF53a mutant cortex, as well as the presence of many cells in the SVZ coexpressing both markers. Both pVIM+ cells and TBR2+ cells in the VZ/SVZ region of BAF53a mutants are positive for H2A histone family member X (H2AX, red), indicating DNA damage (arrowheads). Scale bar, 100 µm. (*E*) Immunofluorescence staining labeling BLBP+ radial glia extending their fibers to the pia (arrowheads, *top* panel), migratory neuroblasts (doublecortin [DCX]), and young and mature neurons (MAP2 and NeuN, respectively) showing mislocalized DCX+ neuroblasts (arrowhead, *bottom* panel) and NEUN+ neurons (arrowheads, *bottom right*) in the VZ and IZ, respectively, in BAF53a mutant cortex. Scale bar, 100 µm. (*F*) E18.5 immunostainings of mouse cortical plate for markers of layer VI (TBR1, green), layer IV-V (CTIP2, blue; SATB2, red), and layer II-III (CUX1, red) excitatory neurons reveal disorganization of deep cortical layers and loss of superficial layers in BAF53a mutant compared with control brains. Scale bar, 100 µm.

ablation of BAF53a in NSPCs leads to deficits in cell cycle progression and disruption of the neurogenic niche. These defects in turn have major consequences on neuronal differentiation, resulting in improper mixing of nascent populations and deficits in the generation of later-born lineages.

Intrinsic and extrinsic drivers of NSPC proliferation cannot rescue cell cycle block resulting from Baf53a *deletion*

A well-known feature of cell cycle exit in the nervous system is that it occurs in the continued presence of extrinsic

drivers of the cell cycle. To determine whether BAF53a operates upstream or downstream from known growth signaling pathways in vivo, we first asked whether β-catenin could promote NSPC cell cycle progression in the absence of BAF53a. WNT signaling is a powerful driver of NSPC expansion, as transgenic expression of constitutively active β-catenin in mice promotes cell cycle re-entry and proliferation of NSPCs and a resulting increase in cortical surface area and brain size (Chenn and Walsh 2002). However, even when β-catenin is constitutively expressed, NSPCs still exit the cell cycle, raising the question of which mechanisms control cell cycle exit under these conditions. Therefore, we bred mice in which the expression of constitutively active β-catenin and deletion of *Baf53a* were both driven by the *Nestin-Cre* transgene, permitting concurrent expression of β-catenin and inactivation of *Baf53a* in NSPCs. As expected, expression of active β-catenin in *Baf53a*$^{fl/+}$ mice resulted in excess NSPC proliferation, as measured by KI67 staining, and a markedly enlarged telencephalon at E15.5 (Fig. 3A,B; Supplemental Fig. S4A,B). However, expression of active β-catenin in *Baf53a*$^{fl/-}$ NSPCs failed to rescue the cell cycle block resulting from *Baf53a* deletion, as reflected by a persistent reduction in the proportion of KI67-expresssing cells in double mutants and accompanying elevated levels of PH3 staining at E15.5. The double mutant brains also remained microcephalic and displayed reduced cortical thickness (Fig. 3A,B; Supplemental Fig. S4A,B).

Growth factors like bFGF and EGF have also been shown to promote NSPC proliferation (Palmer et al. 1995). It is possible that BAF53a-containing BAF complexes control cell cycle progression by driving growth factor production or, alternately, that they operate downstream from growth factors, as in the case of β-catenin. We thus examined whether the cell cycle block at G1/S and G2/M observed in BAF53a mutants could be rescued by extrinsic application of growth factors in vitro. Specifically, we tested whether increasing concentrations of bFGF and EGF in the culture medium could compensate for loss of BAF53a in *Actin-CreER;Baf53a*$^{fl/-}$ NSPCs. Under normal proliferative conditions, EGF and bFGF in the media (20 ng/mL) failed to rescue cell cycle block in NSPCs lacking BAF53a. Addition of fivefold higher concentrations of these two mitogens could partially rescue the block at G1/S but did not rescue the G2/M block (Fig. 3C,D). Transduction of NSPCs with *c-myc*-overexpressing lentiviruses has also been shown to enhance cell proliferation by promoting G1/S progression (Coller et al. 2000; Grandori et al. 2000; Kerosuo et al. 2008); however, in *Actin-CreER;Baf53a*$^{fl/-}$ NSPCs, overexpression of *c-myc* failed to rescue G2/M block resulting from *Baf53a* deletion and only partially rescued the block at G1/S (Fig. 3E,F). In addition, overexpression of *Sox2* and *Pax6*, known regulators of radial glia cell identity and maintenance, increased NSPC proliferation in control cultures but failed to rescue cell cycle block at either G1/S or G2/M in *Baf53a*-deleted NSPCs (Supplemental Fig. S4C,D). Collectively, these studies suggest that BAF53a is necessary for NSPC proliferation and that it functions directly on cell cycle regulatory mechanisms downstream from known intrinsic or extrinsic drivers of proliferation.

BAF53b rescues cell cycle block resulting from deletion of Baf53a

As NSPCs exit the cell cycle in the developing brain, npBAF complexes containing BAF53a, BAF45a/d, and SS18 switch subunits to produce neuron-specific nBAF complexes containing BAF53b, BAF45b/c, and CREST. To determine whether BAF subunit exchange has a causal role during neurogenesis, we sought to determine whether BAF53b expression can rescue the cell cycle block and cell death resulting from *Baf53a* deletion in NSPCs. We hypothesized that BAF53a mutant NSPCs remain blocked in the cell cycle until nBAF subunits are expressed to promote differentiation. We thus attempted to rescue the cell cycle block in mutant NSPCs, not by inducing cell cycle progression and proliferation, but rather by promoting cell cycle exit and neural differentiation. To test this hypothesis in vitro, we used lentiviruses to overexpress either *Baf53a* or *Baf53b* alone in inducible *Actin-CreER;Baf53a*$^{fl/-}$ NSPCs grown in media containing bFGF and EGF (Supplemental Fig. S5A). Following tamoxifen treatment of NSPCs and consistent with our previous findings, we observed a cell cycle block at both G1/S and G2/M in cells lacking BAF53a (Fig. 4A–C). Restoring BAF53a expression rescued the cell cycle block in mutant cells (Fig. 4A,B). Strikingly, cell cycle block in NSPCs lacking BAF53a was also rescued by overexpression of BAF53b (Fig. 4A–C). However, this rescue led to continued proliferation rather than cell cycle exit, suggesting that expression of BAF53b alone, in the absence of the other nBAF subunits, is not sufficient to promote high levels of neural differentiation in vitro. To further explore the fate of cells rescued by either BAF53a or BAF53b overexpression, we immunostained for the NSPC marker NESTIN and the neuronal marker MAP2ab (Supplemental Fig. S5B,C). As expected, the number of NESTIN+ cells was dramatically reduced in BAF53a mutant cultures. Overexpression of BAF53a or BAF53b was sufficient to rescue NESTIN expression (Supplemental Fig. S5D), at least in part owing to increased cell survival (Fig. 4B; Supplemental Fig. S5E). Interestingly, we detected MAP2ab-expressing cells following tamoxifen treatment, even in media containing EGF and bFGF. This suggests that loss of BAF53a is sufficient to promote neuronal differentiation of NSPCs and may be required for NSPCs to stop responding to extrinsic proliferative signals and initiate differentiation programs. MAP2ab expression further increased with overexpression of BAF53b (Supplemental Fig. S5D), in line with the idea that subunit switching enables differentiation onset. Together, these data indicate that, in this in vitro experimental setting, overexpression of BAF53b alone is sufficient to rescue the cell cycle block resulting from *Baf53a* deletion but not to promote high levels of cell cycle exit and neural differentiation. This may be in part explained by the fact that the other two nBAF subunits are not overexpressed in these rescue

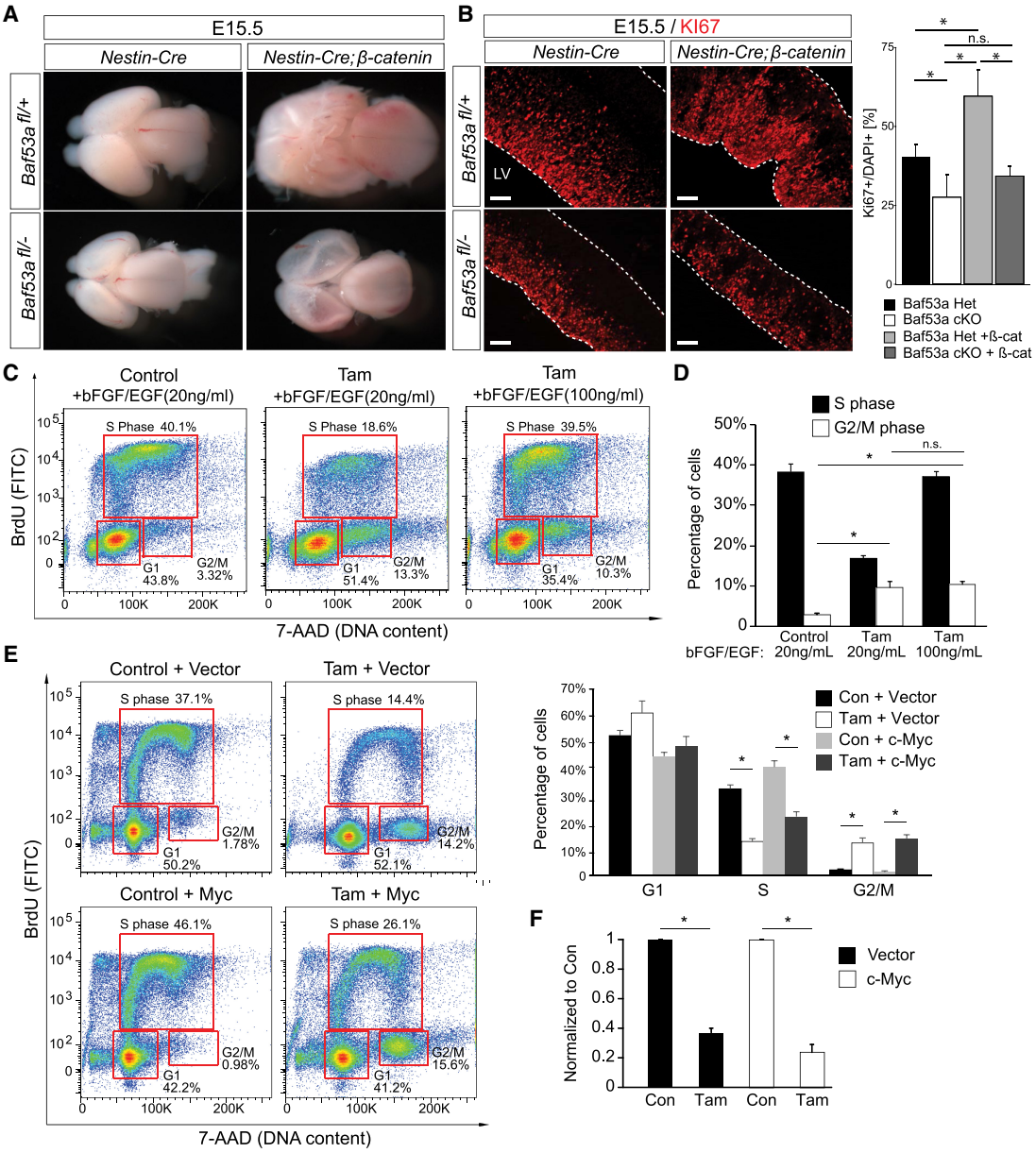

Figure 3. Intrinsic and extrinsic drivers of NSPC proliferation cannot rescue proliferation defects resulting from *Baf53a* deletion. (*A*) Photomicrographs of whole brains from BAF53a mutant or control embryos with and without the *β-catenin* transgene at E15.5. (*B*) Immunofluorescence staining for the proliferation marker KI67 on E15.5 sagittal sections through the cortex of BAF53a mutant or control embryos with and without the *β-catenin* transgene, respectively. Scale bar, 100 µm. Quantification of the percentage of KI67+/DAPI+ cells in the four genotypes. $n = 3$–5 embryos per genotype. Data presented as mean ± SEM. (*) $P < 0.05$, one-way ANOVA and post-hoc Tukey's test for multiple comparisons. (*C*) Cell cycle FACS analysis of *Actin-CreER*; *Baf53a*$^{fl/-}$ neurospheres upon BrdU incorporation with and without tamoxifen (Tam) treatment and following application of increasing concentrations of the growth factors bFGF and EGF. (*D*) Quantification of the mitogens' effects on cell cycle in the context of *Baf53a* deletion. $n = 3$. Error bars represent SEM. (*) $P < 0.05$. (*E*) Cell cycle FACS analysis depicting the effect of c-*Myc* overexpression in *Actin-CreER*; *Baf53a*$^{fl/-}$ neurospheres with and without tamoxifen. Cells were infected with either empty vector virus or c-*Myc* virus and selected by hygromycin prior to tamoxifen treatment for 72 h. $n = 3$. Error bars represent SEM. (*) $P < 0.05$. (*F*) Quantification of total cell numbers 72 h after tamoxifen treatment (normalized to condition treated with EtOH). $n = 3$. Error bars represent SEM. (*) $P < 0.05$.

experiments. In these studies, therefore, BAF53b may be interacting with npBAF subunits to promote cell cycle progression.

To test the role of all three nBAF subunits in vivo, we used in utero electroporation to introduce vectors expressing *Baf53b*, *Baf45b*, and *Crest* (nBAF) into BAF53a mutant and control cortices at E13.5. To evaluate the percentage of electroporated NSPCs that exit the cell cycle (quit fraction), pregnant dams received an injection of BrdU at E14.5 (24 h prior to sacrifice), and embryonic brains were

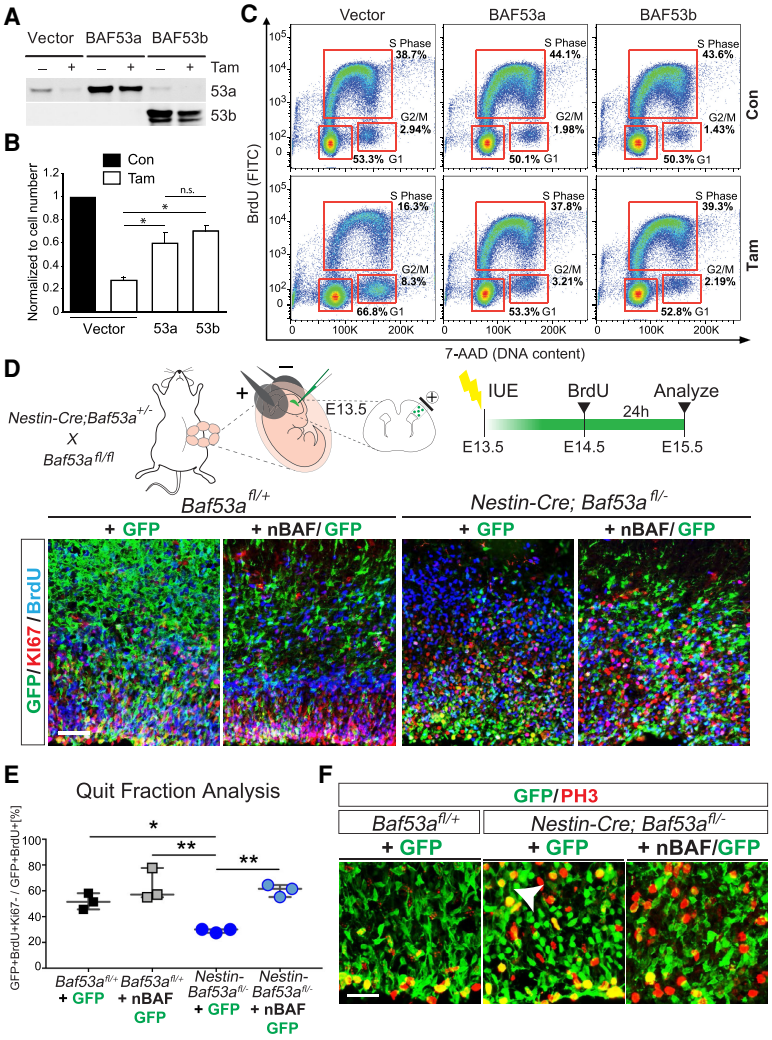

Figure 4. BAF53b can rescue cell cycle block resulting from *Baf53a* deletion in vitro and in vivo. (*A*) Western blot analysis to measure BAF53a and BAF53b levels in *Actin-CreER;Baf53a*$^{fl/-}$ neurospheres treated with tamoxifen or vehicle following infection with empty vector or *Baf53a*- or *Baf53b*-overexpressing lentiviruses. (*B*) Quantification of *Actin-CreER;Baf53a*$^{fl/-}$ total cell numbers 72 h after tamoxifen treatment (normalized to control condition infected with empty vector and treated with EtOH). $n = 3$. Error bars represent SEM. (*) $P < 0.05$. (*C*) Cell cycle FACS analysis of *Actin-CreER; Baf53a*$^{fl/-}$ neurospheres treated with tamoxifen or vehicle (EtOH) infected with empty vector or *Baf53a*- or *Baf53b*-overexpressing lentiviruses. Cells were selected by puromycin prior to tamoxifen treatment. Infected cells were labeled with BrdU for 2 h prior to FACS analysis 72 h after tamoxifen administration. (*D*) Schematic of experimental paradigm: in utero electroporation (IUE) of BAF53a mutant and control E13.5 embryos with a control plasmid (GFP), or a mix of GFP and a polycistronic vector coexpressing *Baf53b*, *CREST*, and *Baf45b* (nBAF). Representative images of coronal sections from E15.5 control *Baf53a*$^{fl/+}$ and *Nestin-Cre; Baf53a*$^{fl/-}$ mutant brains immunostained for GFP (green), KI67 (red), and BrdU (blue). Scale bars, 50 µm. (*E*) Cell cycle exit analysis of BAF53a mutant and control brains at E15.5 following electroporation with control (GFP) or nBAF vectors ($n = 3$ embryos per condition). Data presented as mean ± SEM. (*) $P < 0.03$, (**) $P < 0.004$, one-way ANOVA and post-hoc Tukey's test for multiple comparisons. (*F*) Immunofluorescence staining of coronal sections through the VZ/SVZ of electroporated BAF53a mutant and control E15.5 embryos showing a multitude of hypertrophic GFP-electroporated (green) cells in BAF53a mutant brains that coexpress the M-phase marker PH3 (red; white arrow; *middle* panel). In the *right* panel, the number of yellow cells is dramatically reduced as nBAF-expressing cells (green) exit the cell cycle and are no longer PH3-positive (red). Scale bars, 25 µm.

analyzed at E15.5 (Fig. 4D). BAF53a mutant mice electroporated with a control GFP construct displayed a significantly reduced quit fraction compared with control mice, consistent with the observed cell cycle block following *Baf53a* deletion in NSPCs. Electroporating BAF53a mutant mice with constructs expressing the nBAF subunits successfully rescued the quit fraction deficit (Fig. 4E). The majority of nBAF-expressing mutant cells also no longer expressed PH3 (Fig. 4F), supporting the idea that expression of the nBAF subunits rescues cell cycle block (specifically G2/M arrest) in BAF53a mutant mice and contributes to cell cycle exit. In a series of control experiments, we also used in utero electroporation to overexpress nBAF- and npBAF-specific subunits in wild-type mice, to determine whether prolonged npBAF expression or premature nBAF expression was sufficient to alter the timing of cell cycle exit (Supplemental Fig. 6A). We did not observe any significant differences in quit fraction with any of these manipulations compared with GFP-only control electroporations (Supplemental Fig. S6A,B), suggesting that BAF53a repression is required to initiate subunit switching and differentiation. These striking results underline the contribution of BAF subunit switching to cell cycle exit in the developing cortex. BAF53a is required to maintain cell cycle progression, and its suppression leads to cell cycle arrest. The overexpression of nBAF subunits is able to rescue the loss of BAF53a, releasing cell cycle blockade by promoting cell cycle exit and the acquisition of specific neural fates.

BAF53a regulates cell cycle genes in the developing cortex

Chromatin remodelers regulate the epigenetic landscapes that establish cell type-specific gene expression patterns (Ho and Crabtree 2010). To identify BAF53a-dependent target genes, we performed RNA-sequencing on E15.5 forebrains isolated from four control (*Nestin-Cre; Baf53a*$^{fl/+}$) and four mutant (*Nestin-Cre;Baf53a*$^{fl/-}$) mice. To determine significantly regulated genes, we applied a fold change cutoff of 1.5× and a significance threshold of FDR < 0.1 (Fig. 5A). The sample-to-sample clustering and

PCA analysis revealed that the data sets were highly reproducible, as they strongly clustered by genotype (Fig. 5B,C). Using these criteria, we identified 388 genes with increased expression and 200 genes with reduced expression in BAF53a mutant brains (Fig. 5D). Using the DAVID software, we analyzed the 588 differentially expressed genes (DEGs) to associate gene ontology (GO) terms enriched in the data set (Fig. 5E). Down-regulated genes were strongly enriched for GO terms associated with cell division, cell cycle, and transcriptional regulation, whereas up-regulated genes were enriched for GO terms such as cell adhesion, ion transport, axon guidance, cell migration, and brain development, suggesting that deletion of *Baf53a* both suppresses the cell cycle and promotes neural differentiation. Key cell cycle genes, such as *Ccng1*, *Ndc80*, *Ttk*, and *Nusap1*, which regulate G2/M progression, were down-regulated in mutant brains, as was the radial glial marker *Prom1*. Genes expressed in interneurons (e.g., *Dlx1*, *Dlx6*, and *Lhx6*), which migrate into the cortex from ventral telencephalic germinal zones, are also markedly reduced in expression upon *Baf53a* deletion, suggesting impaired differentiation of those populations in mutant mice. Furthermore, genes expressed in later-born excitatory neuronal populations and genes associated with glial differentiation, such as *Cux2*, *Pdgfra*, and *Olig2*, were reduced in the absence of BAF53a. Immunostaining for glial lineages supported these findings, revealing an almost complete absence of OLIG2-expressing oligodendrocyte progenitors, as well as depletion and displacement of BLBP- and SOX9-expressing progenitors in mutant mouse cortices (Supplemental Fig. S6C,D). These data strongly support the phenotypic analysis we performed on BAF53a mutant brains and suggest that BAF53a regulates genes involved in cell cycle regulation in the developing brain.

BAF53a regulates chromatin accessibility at neural enhancers

BAF chromatin remodeling complexes are thought to regulate gene expression by influencing chromatin accessibility at specific genomic loci (Ho et al. 2009). To

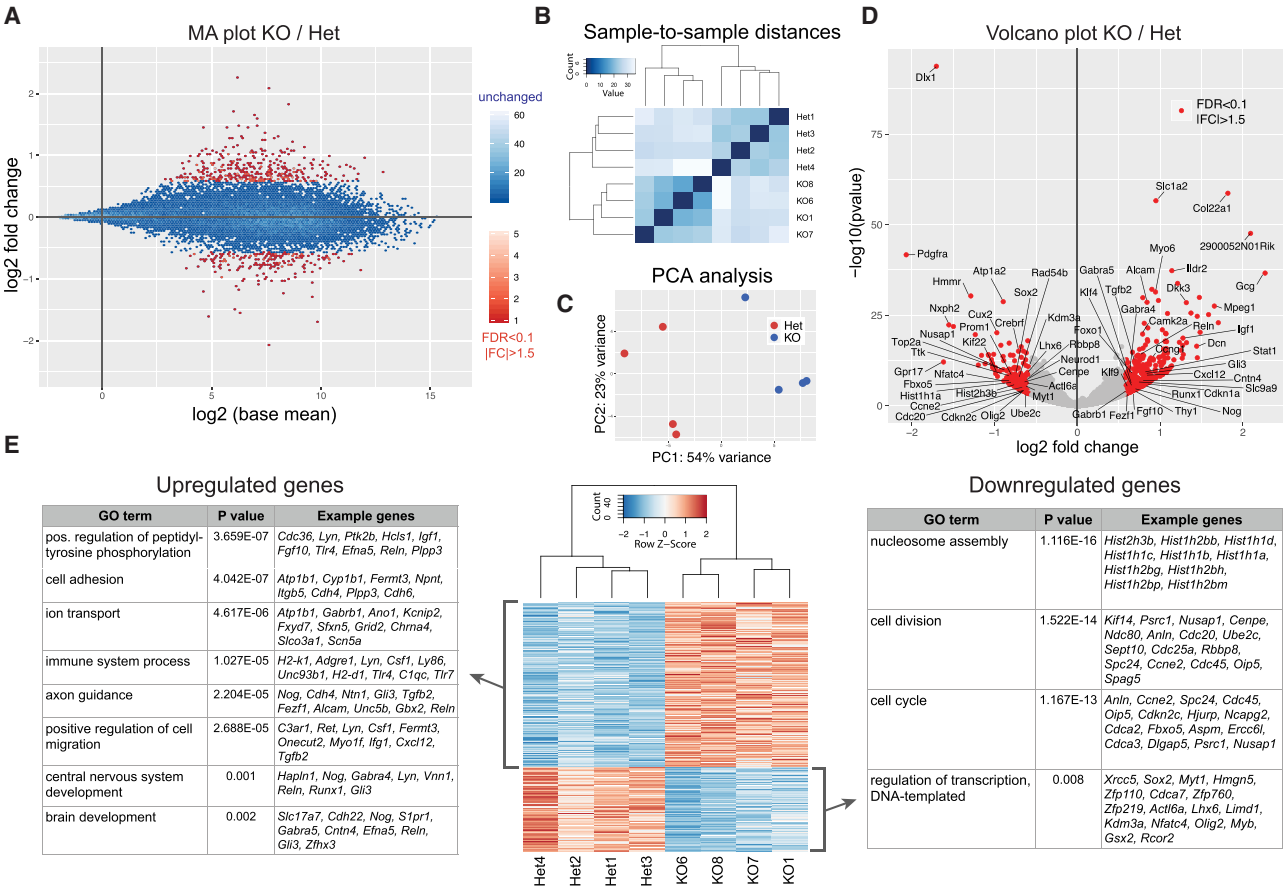

Upregulated genes

GO term	P value	Example genes
pos. regulation of peptidyl-tyrosine phosphorylation	3.659E-07	*Cdc36, Lyn, Ptk2b, Hcls1, Igf1, Fgf10, Tlr4, Efna5, Reln, Plpp3*
cell adhesion	4.042E-07	*Atp1b1, Cyp1b1, Fermt3, Npnt, Itgb5, Cdh4, Plpp3, Cdh6,*
ion transport	4.617E-06	*Atp1b1, Gabrb1, Ano1, Kcnip2, Fxyd7, Sfxn5, Grid2, Chrna4, Slco3a1, Scn5a*
immune system process	1.027E-05	*H2-k1, Adgre1, Lyn, Csf1, Ly86, Unc93b1, H2-d1, Tlr4, C1qc, Tlr7*
axon guidance	2.204E-05	*Nog, Cdh4, Ntn1, Gli3, Tgfb2, Fezf1, Alcam, Unc5b, Gbx2, Reln*
positive regulation of cell migration	2.688E-05	*C3ar1, Ret, Lyn, Csf1, Fermt3, Onecut2, Myo1f, Ifg1, Cxcl12, Tgfb2*
central nervous system development	0.001	*Hapln1, Nog, Gabra4, Lyn, Vnn1, Reln, Runx1, Gli3*
brain development	0.002	*Slc17a7, Cdh22, Nog, S1pr1, Gabra5, Cntn4, Efna5, Reln, Gli3, Zfhx3*

Downregulated genes

GO term	P value	Example genes
nucleosome assembly	1.116E-16	*Hist2h3b, Hist1h2bb, Hist1h1d, Hist1h1c, Hist1h1b, Hist1h1a, Hist1h2bg, Hist1h2bh, Hist1h2bp, Hist1h2bm*
cell division	1.522E-14	*Kif14, Psrc1, Nusap1, Cenpe, Ndc80, Anln, Cdc20, Ube2c, Sept10, Cdc25a, Rbbp8, Spc24, Ccne2, Cdc45, Oip5, Spag5*
cell cycle	1.167E-13	*Anln, Ccne2, Spc24, Cdc45, Oip5, Cdkn2c, Hjurp, Ncapg2, Cdca2, Fbxo5, Aspm, Ercc6l, Cdca3, Dlgap5, Psrc1, Nusap1*
regulation of transcription, DNA-templated	0.008	*Xrcc5, Sox2, Myt1, Hmgn5, Zfp110, Cdca7, Zfp760, Zfp219, Actl6a, Lhx6, Limd1, Kdm3a, Nfatc4, Olig2, Myb, Gsx2, Rcor2*

Figure 5. Loss of BAF53a leads to reduced expression of cell cycle regulators and enhanced expression of differentiation genes. (*A*) Genome-wide gene expression changes measured by RNA-seq in BAF53a mutant (*Nestin-Cre;Baf53a*$^{fl/-}$, KO) and heterozygous control (*Nestin-Cre;Baf53a*$^{fl/+}$, Het) forebrains at E15.5 ($n = 4$). Magnitude and average (MA) plot (KO/Het) of RNA-seq data, displaying significantly changed genes in red (FDR < 0.1 and fold change > 1.5). (*B*) Sample-to-sample distance matrix reveals clustering of Het and KO replicates. (*C*) PCA plot highlighting reproducibility of biological replicates that cluster according to genotypes. (*D*) Volcano plot (KO/Het) with a subset of significantly up-regulated and down-regulated genes labeled in red. (*E*) Heat map of significantly up-regulated and down-regulated genes as well as gene ontology (GO) terms of biological processes associated with these genes.

determine the direct effects of *Baf53a* deletion on chromatin accessibility genome-wide, we performed ATAC-seq analysis on four control (*Nestin-Cre;Baf53a*$^{fl/+}$) and four mutant (*Nestin-Cre;Baf53a*$^{fl/-}$) forebrains. We found that 2521 accessible peaks were significantly changed (FDR < 0.1 and fold change cutoff of 1.5×), representing 7% of the total number of accessible peaks in E15.5 forebrains across the genome (Fig. 6A–D). Using GREAT software to associate these *cis*-regulatory regions with specific genes, we associated significantly regulated ATAC peaks to 3153 genes. Among this list of genes, 151 were also differentially expressed in our RNA-seq analysis (representing 25.6% of the 588 DEGs). This seemingly low correlation between accessibility measured by ATAC-seq and gene expression measured by RNA-seq has also been observed in several other studies (Klemm et al. 2019). However, GO term analysis revealed striking similarities with the results of our RNA-seq analysis (Fig. 6E, F). Lost accessibility peaks were associated with GO terms such as neuron fate commitment, stem cell maintenance, maintenance of cell number, and regulation of Notch signaling. This finding is in line with our phenotypic analysis of NSPCs in BAF53a mutant mice and reveals that BAF53a controls accessibility at discrete regulatory regions associated with genes that control NSPC identity and numbers, such as *Pax6*, *Sox2*, *Ascl1*, *Notch1*, and *Hes1* (Fig. 6G). We also found that accessibility was decreased at specific regulatory regions associated with gliogenesis genes (*Olig1/2* and *Nkx6-2*), interneuron genes (*Dlx1/2*), and upper-layer neuron genes (*Brn2*), consistent with our RNA sequencing data and immunostaining for markers of these cell types in BAF53a mutant brains. In contrast, gained accessibility peaks were associated with GO terms such as neuron development and differentiation, axon guidance, and neuron projection guidance. This observation is in line with our phenotypic analysis demonstrating premature induction of neuronal differentiation in BAF53a mutant cortices at E15.5 (Fig. 2E). Increased NEUN staining in mutant brains is accompanied by increased accessibility at discrete regulatory regions associated with neuronal genes, including *Map2*, *Bdnf*, *Robo2*, and *Dcc* (Fig. 6H). We also performed a chromatin feature analysis using ChromHMM software to characterize chromatin states at the ATAC peaks. We found that the majority of BAF53a-dependent ATAC peaks were at neural enhancers (Enh) characterized by H3K4me1, H3K9ac, and H3K27ac histone modifications in E15.5 forebrains (Fig. 6F). These results suggest that BAF53a-containing npBAF complexes directly influence accessibility to forebrain enhancers that regulate the expression of genes involved in NSPC maintenance and the onset of neural differentiation.

BAF complexes regulate accessibility at neurogenesis transcription factor (TF) binding sites by opposing Polycomb-mediated repression

Changes in BAF53a-dependent accessibility were often found at discrete enhancer sequences rather than across all accessible regulatory regions associated with a given target gene (Fig. 6G,H). This suggested that accessibility at specific motifs may be regulated by the BAF complex in the developing forebrain. Motif analysis programs generally detect only the sequence motif for a given TF but do not detect changes in occupancy induced by a genetic or environmental modification. A recently developed technique, however, allows one to identify changes in TF activity (BaGFoot), and we applied this method of analysis to the BAF53a target genes identified by ATAC-seq. Using BaGFoot analysis to determine both changes in flanking accessibility as well as changes in TF footprints, we found that members of the ASC, SOX, OLIG, BRN, and PAX families of TFs displayed reduced activity in BAF53a mutant brains (Fig. 7A). Using published ChIP-seq data sets from mouse NSPCs for four representative proneural TFs in these families (ASCL1, SOX2, OLIG2, and PAX6) (Wapinski et al. 2013; Mistri et al. 2015; Nishi et al. 2015; Sun et al. 2015), we also found that their binding was enriched in ATAC-seq peaks down-regulated in BAF53a cKO forebrains (Fig. 7B). Next, we associated the ChIP-seq peaks from each data set with corresponding genes and found that the vast majority of the 151 genes that showed both changes in expression (by RNA-seq) and chromatin accessibility (by ATAC-seq) were also targets of ASCL1, SOX2, and OLIG2 TFs (Supplemental Fig. S7A,B). For example, *Htr3a* expression is decreased in BAF53a cKO forebrains, and chromatin accessibility is also decreased at neighboring regulatory sequences. These regulatory regions correspond to ASCL1, SOX, and OLIG2 peaks. Interestingly, the TF binding sites are not all always found across all the regulated ATAC peaks but rather at different subsets. Consistent with this, ASCL1 motifs displayed reduced accessibility in BAF53a cKO forebrains compared with controls (Fig. 7C). Furthermore, HOMER analysis revealed that ASCL1, BRN2, and SOX motifs were enriched in the peaks that displayed decreased accessibility upon loss of BAF53a (Supplemental Fig. S7C). SOX2, strongly expressed in radial glia, is a key regulator of cortical NSPC maintenance and proliferation (Graham et al. 2003). ASCL1 and BRN2 TFs also regulate progenitor proliferation and neuronal production during brain development (Bertrand et al. 2002; Castro et al. 2006). Moreover, the combination of MYT1L, ASCL1, and BRN2 can reprogram cellular identity and convert fibroblasts into neurons (Vierbuchen et al. 2010), further highlighting their role in neuronal differentiation. Interestingly, suppression of BAF53a in fibroblasts with *miR-9/miR-124* reprograms human fibroblasts to neurons without a need for ASLC1 overexpression (Victor et al. 2014). Collectively, these data lead us to propose that BAF53a is required to generate accessibility for neurogenic TFs to bind specific motifs and regulate target genes during forebrain development.

Finally, we sought to determine the molecular mechanism through which BAF53a-containing BAF complexes regulate accessibility at these sites to control the expression of genes involved in maintaining NSPC identity and cell cycle progression. In mouse ES cells and fibroblasts, BAF promotes chromatin accessibility at enhancers and bivalent genes through eviction of the Polycomb

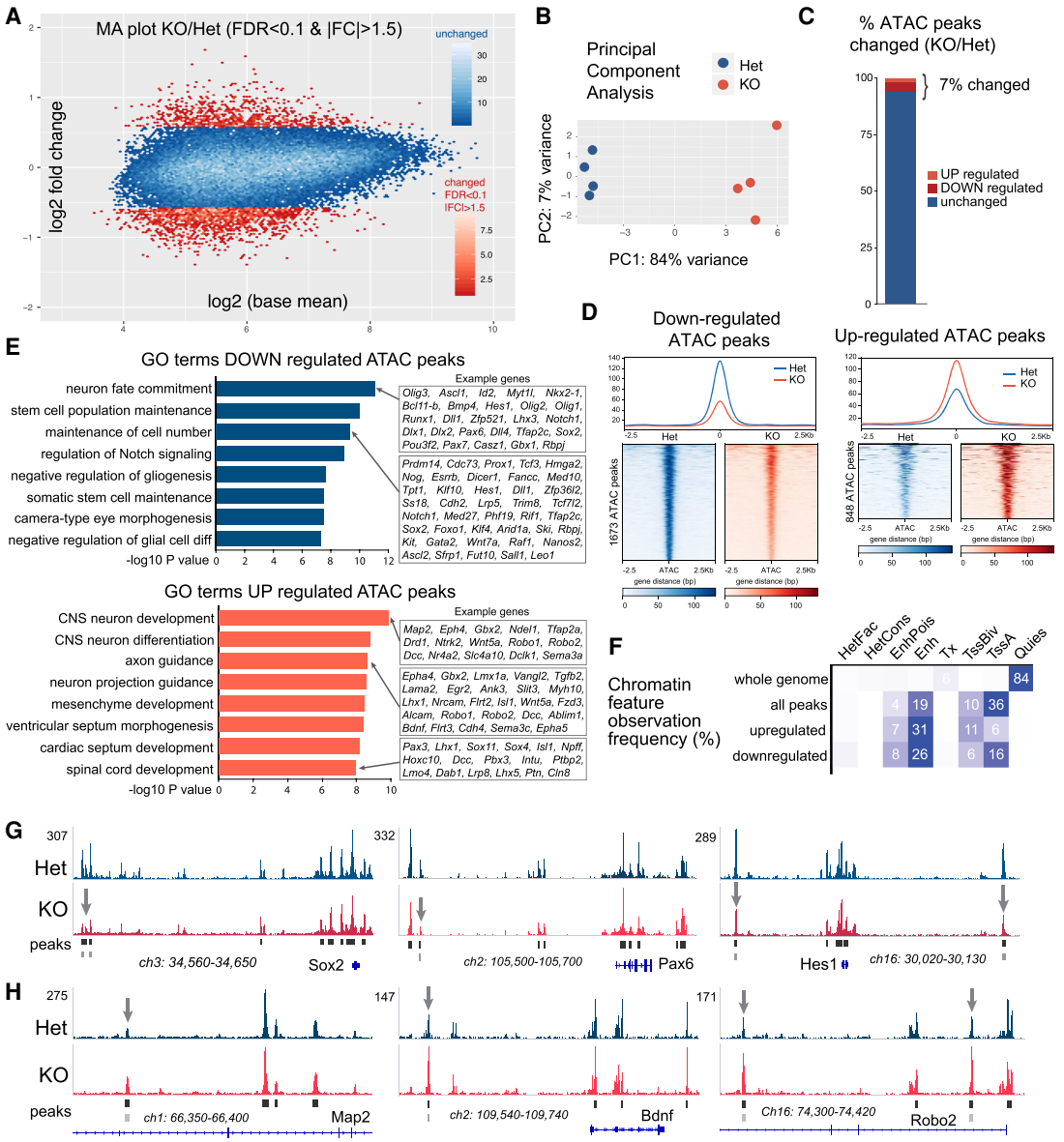

Figure 6. BAF53a regulates chromatin accessibility at NSPC identity and neural differentiation genes. (*A*) Genome-wide chromatin accessibility changes as measured by ATAC-seq in BAF53a mutant (*Nestin-Cre*;*Baf53a*$^{fl/-}$, KO) and heterozygous control (*Nestin-Cre*;*Baf53a*$^{fl/+}$, Het) forebrains at E15.5 ($n = 4$). Magnitude and average (MA) plot (KO/Het) of ATAC-seq data, displaying significantly changed peaks in red (FDR < 0.1 and fold change > 1.5). (*B*) PCA plot highlighting reproducibility of biological replicates that cluster according to genotypes. (*C*) Percentage of the total 39,041 ATAC peaks that are up-regulated or down-regulated. (*D*) Genome-wide accessibility profiles at up-regulated and down-regulated ATAC peaks in *BAF53a* KO and Het forebrains. (*E*) Analysis of gene ontology (GO) terms of biological processes associated with the genes that display gains or losses in accessibility in regulatory elements that control their expression. GREAT software was used to associate ATAC peak with a given gene. (*F*) Chromatin feature analysis reveals frequency of accessibility changes (percentage) according to specific regulatory elements. The peaks that display changes in accessibility are most frequently associated with enhancer elements (Enh: H3K4me1, H3K9ac, and H3K27ac). ChromHMM was used to determine chromatin features using Encode data from E15 mouse forebrains (ChIP-seq: H3K4me3, H3K4me2, H3K4me1, H3K36me3, H3K9ac, H3K27ac, H3K27me3, and H3K9me3). (*G*,*H*) Representative genome browser tracks showing changes in accessibility peaks in KO and Het forebrains at regulators of NSPC identity and neural differentiation.

repressive complex 2 (PRC2), which places the repressive H3K27me3 histone modification to repress gene expression (Braun et al. 2017; Kadoch et al. 2017; Stanton et al. 2017). We thus analyzed BRG1 and H3K27me3 ChIP-seq data from wild-type forebrains and determined the overlap with the ATAC peaks measured in our data sets. We found that the majority of accessible peaks overlapped with peaks bound by BRG1, whereas very few accessible peaks were marked with H3K27me3 (Fig. 7D). This suggests that BAF complexes may generate

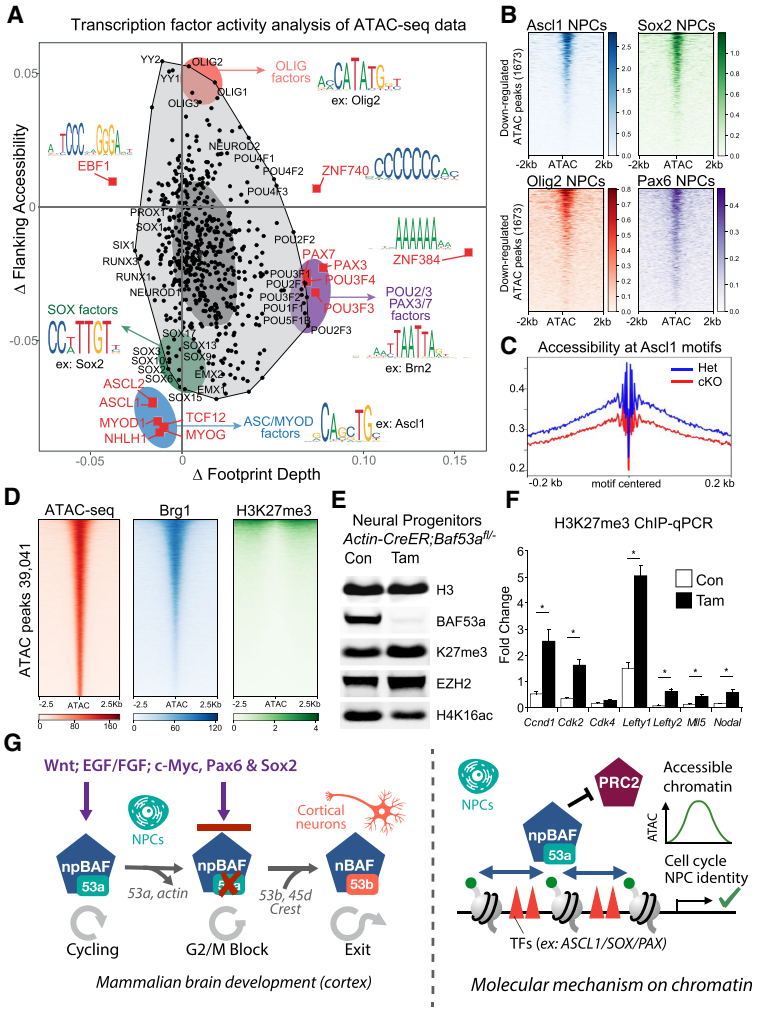

Figure 7. BAF53a regulates accessibility for neurogenesis TF activity through opposition to Polycomb repressive complex 2. (*A*) BaGFoot analysis of TF activity at BAF53a-dependent ATAC peaks. This analysis determines both changes in flanking accessibility, as well as changes in TF footprints. ASC, SOX, BRN, and PAX families of TFs displayed reduced activity in BAF53a mutant brains. TF binding motifs for a given member of each family are displayed as examples. (*B*) Analysis of neural TF binding at ATAC-seq peaks down-regulated in BA53a mutant (cKO) forebrains. We used published ChIP-seq data sets from mouse NPCs for ASCL1 (Wapinski et al. 2013), SOX2 (Mistri et al. 2015), OLIG2 (Nishi et al. 2015), and PAX6 (Sun et al. 2015) to show binding of these different TFs at BAF53a-dependent accessibility peaks. (*C*) Characterization of ATAC peaks at ASCL1 motifs in BAF53a mutant (cKO) and control (Het) forebrains at E15.5. Chromatin accessibility is reduced at ASCL1 motifs in mutant brains. (*D*) Analysis of ChIP-seq and ATAC-seq data sets to characterize BRG1 and H3K27me3 levels across accessibility peaks in wild-type mouse forebrains. The majority of accessible regions are bound by BRG1, whereas very few accessible regions are marked with H3K27me3. (*E*) Western blot analysis of H3K27me3 levels in *Actin-CreER;Baf53a*$^{fl/-}$ NSPCs treated with tamoxifen for 72 h. (*F*) ChIP-qPCR analysis of H3K27me3 levels at cell cycle regulator genes, stem/progenitor cell maintenance genes, and *Hox* cluster genes. The levels of the H3K27me3 repressive marks are increased at cell cycle genes following *Baf53a* deletion in *Actin-CreER;Baf53a*$^{fl/-}$ NSPCs. $n = 3$. Error bars represent SEM. (*) $P < 0.05$. (*G*) During cortical development, the switch from npBAF to nBAF chromatin regulators enables cell cycle exit and ensures faithful initiation and execution of postmitotic neural differentiation programs in the cortex. (*Left* panel) Continued expression of BAF53a-containing npBAF complexes in NSPCs promotes proliferation downstream from multiple cues (e.g., WNT and EGF/bFGF) by opposing the actions of PRC2, generating chromatin accessibility for cell type-specific TFs to drive expression of cell cycle and NSPC identity genes. When the npBAF subunit BAF53a is deleted, NSPCs can no longer respond to proproliferative signals and await expression of BAF53b and the other nBAF subunits to progress through neural differentiation programs. (*Right* panel) npBAF complexes regulate chromatin accessibility at cell cycle genes and NPC identity genes through opposition to repressive Polycomb complexes. (*Right* panel) The chromatin accessibility generated by npBAF remodeling complexes promotes the binding activity of neural identity TFs, including the pioneer TFs ASCL1 and SOX2.

accessible chromatin in the developing forebrain by restricting the placement of H3K27me3 by PRC2 complexes. To test this idea, we measured H3K27me3 levels in NSPCs lacking BAF53a. We found that *Baf53a* deletion led to increased global levels of H3K27me3 in cultured cells, as well as in the developing cortex at E15.5 (Fig. 7E; Supplemental Fig. S7F). Moreover, we performed H3K27me3 ChIP experiments in BAF53a mutant cells and found that H3K27me3 levels were increased at cell cycle genes (*Ccdn1*, *Cdk2*, and *Cdk4*) (Fig. 7F). ChIP experiments for PRC2 complex subunits SUZ12 and EZH2 revealed similar increases at cell cycle genes and stem cell identity genes following *Baf53a* deletion (Supplemental Fig. 7D,E). Together, these results suggest that BAF53a is required for npBAF complexes to promote accessibility for TF binding by directly opposing Polycomb (Fig. 7G).

Discussion

Our studies indicate that the npBAF to nBAF switch promotes the exit of NSPCs from the cell cycle in the embryonic brain, acting downstream from other recognized regulators of NSPC proliferation, thereby providing an explanation for how NSPCs exit the cell cycle in the presence of continued growth signals. The three key findings of our study are that (1) BAF53a-containing npBAF complexes directly regulate accessibility at genes required for normal cell cycle progression and NSPC maintenance, including targets of proneural and "pioneer" TFs like SOX2, (2) suppression of BAF53a contributes to NSPC cell cycle exit and differentiation onset, and (3) intrinsic and extrinsic mechanisms that normally regulate NSPC proliferation cannot drive proliferation in the absence of BAF53a, whereas nBAF subunits, which normally replace

BAF53a and the other npBAF subunits, can overcome this cell cycle block by promoting differentiation (Fig. 7G). These observations lead us to propose that BAF53a-containing npBAF complexes are essential for NSPC proliferation and that timely regulation of BAF subunit composition during normal neural development acts as a decisive signal during cell cycle progression.

Proliferation in the developing nervous system involves the convergence of environmental cues and genetic programs balancing NSPC maintenance with cell cycle exit. The precise mechanisms allowing NSPCs to stop responding to proproliferative signals within their environment and instead exit the cell cycle have remained unclear. We sought to identify intrinsic molecular mechanisms that act to directly coordinate cell cycle exit in the developing cortex. Earlier studies suggested roles for npBAF complexes in NSPC proliferation and set the stage for our hypothesis that BAF subunit switching drives cell cycle exit during corticogenesis. Brain-specific deletion of core BAF subunits BRG1 or BAF170 results in opposing phenotypes with respect to cortical thickness (Lessard et al. 2007; Tuoc et al. 2017), suggesting that BAF complexes dynamically control brain size and neuronal content through the expression of specific subunits. npBAF complexes containing BAF53a have been proposed to influence cell cycle maintenance in multiple cell types, as deletion of *Baf53a* leads to cell cycle exit in ES cells, hematopoietic stem cells, and keratinocytes (Aizawa et al. 2004; Yoo et al. 2011; Krasteva et al. 2012; Zhu et al. 2017). This points to npBAF complexes as key molecular players in the maintenance and output of different tissue-specific stem/progenitor cell compartments.

The cellular mechanisms by which npBAF complexes regulate proliferation have to date been poorly understood. Our genomic studies indicate that npBAF complexes containing BAF53a play a fundamental programmatic role in controlling NSPC cell cycle progression, by directly operating on genes that regulate both the G1/S transition as well as progression through G2/M. Deletion of *Baf53a* leads to cell cycle arrest at both G1/S and G2/M, characterized in vivo by a marked disorganization of the germinal zones accompanied by cell death and a dramatic increase in PH3+ cells throughout the VZ/SVZ. Following *Baf53a* deletion, the expression of a number of genes involved in G2/M progression, including *Ccng1, Ndc80*, *Ttk*, *Nusap1*, and the haploid insufficient *Cenpe,* is coordinately altered (Mao et al. 2003). It should be noted that BAF53a protein loss occurred slowly over 2–3 d after CRE-mediated deletion of *Baf53a*, making it difficult to know from the RNA-seq experiments at E15.5 which genes are directly regulated by BAF53a. Nevertheless, owing to these coordinated alterations in the expression of mitotic checkpoint genes and the essential role of BAF complexes in topoisomerase II function (Dykhuizen et al. 2013), we propose that the increased PH3+ cells we observe throughout the germinal zones of BAF53a mutant mice reflects a failure to pass the decatenation mitotic checkpoint. In other cell types, deletion of BAF subunits leads to G2/M arrest due to an inability of Topo-IIa to decatenate DNA prior to M-phase (Dykhuizen et al. 2013). Consistent with such a mechanism and activation of the decatenation checkpoint, we found that deletion of *Baf53a* results in increased anaphase bridges. We also observed reduced expression of genes encoding members of the condensin complex, which has previously been associated with microcephaly and decatenation defects at mitosis (Martin et al. 2016). Failure to pass this checkpoint could also potentially disrupt inter-kinetic nuclear migration of dividing radial glial cells, whose nuclei normally descend to the ventricular surface during G2 to undergo mitosis. In line with this, we observed displaced mitotic PH3+ and pVIM+ radial glia away from the ventricle in mutant brains. Finally, if the decatenation checkpoint is not resolved, cells undergo apoptosis, highlighted by increased cleaved caspase 3 staining in BAF53a mutant brains.

Various intrinsic and extrinsic niche-dependent factors can promote NSPC proliferation. Some of the proteins transducing these signals, for example, β-catenin, have also been reported to interact with BAF complexes (Barker et al. 2001; Vasileiou et al. 2015). We reasoned that manipulating these factors in the context of *Baf53a* deletion would enable us to determine whether BAF53a acts downstream from known proliferative signals. None of the factors that we tested could fully rescue the G1/S block upon *Baf53a* deletion, and all failed to rescue G2/M arrest. This observation suggests that repression of BAF53a and the resulting changes in gene expression, even in the presence of other proliferative signals, allows NSPCs to reduce their responsiveness to mitogenic factors and faithfully exit the cell cycle following the G2/M transition. This idea is in line with previous studies suggesting that the responsiveness of intermediate progenitors to environmental cues is diminished after G2/M (McConnell and Kaznowski 1991; Oberst et al. 2019) and is supported by the upregulation of neural differentiation genes upon *Baf53a* deletion, including *Camk2a* and *Fezf1* (Shimizu et al. 2010), as well as the coordinated changes in chromatin accessibility revealed by our ATAC-seq analyses. *Baf53a* deletion results in decreased accessibility at genes associated with maintaining NSPC identity (e.g., *Pax6, Hes1,* and *Sox2*) and concomitant increases in accessibility at genes associated with neuronal differentiation (e.g., *Map2* and *Ptbp2*) and axon development (e.g., *Wnt5a* and *Nrcam*). Moreover, in ATAC peaks displaying decreased accessibility upon *Baf53a* deletion, we found an enrichment in TF motifs associated with NSPC maintenance and proliferation, including SOX2 and ASCL1 (Bertrand et al. 2002; Graham et al. 2003). These data suggest that *Baf53a* deletion may set differentiation programs in motion by directly regulating accessibility of neural TF motifs and are reinforced by the increased MAP2ab staining we observe upon *Baf53a* deletion in vitro, as well as increased NEUN staining observed in BAF53a mutant cortices in vivo. Importantly, both in vitro and in vivo, expression of BAF53b alone or in combination with other nBAF subunits is sufficient to rescue cell cycle block. Introducing BAF53b alone into BAF53a mutant cells in vitro promotes continued proliferation, presumably owing to BAF53b associating with npBAF subunits in the absence

of its nBAF partners. Expression of all three nBAF subunits in BAF53a mutant NSPCs in vivo, on the other hand, contributes to their exit from the cell cycle. It is also possible that, in this in vivo milieu, exogenously expressed nBAF complexes could have an opportunity to interact with progenitor-specific transcription factors different from their normal partners, thereby adopting some npBAF functions in addition to the nBAF function of contributing to cell cycle exit. Our observations support the model that repression of BAF53a normally induces cell cycle exit, and when BAF53b and the other nBAF subunits are incorporated into BAF complexes, neuronal differentiation programs are consolidated and allowed to progress. Expression of nBAF subunits in wild-type mice does not alter cell cycle exit, implying that repression of BAF53a is required to initiate subunit switching and differentiation, but premature inactivation of BAF53a, as in our mutant mice, leads to a premature block in cell cycle progression. These data are consistent with earlier studies showing that postmitotic nBAF complexes do not regulate cell cycle genes, instead targeting genes involved in neuronal function (Wu et al. 2007; Vogel-Ciernia et al. 2013). Together, our findings lead us to propose that cell type-specific BAF complexes regulate the emergence of distinct neural cell fates by generating chromatin accessibility for cell type-specific TF activity.

We have shown that the BAF complex regulates cell cycle progression in the developing brain by shaping chromatin accessibility at genes controlling NSPC proliferation and differentiation. How do BAF53a-containing npBAF complexes orchestrate these coordinated gene expression changes to promote proliferation? In BAF53a mutant cortices, we observed a significant increase in the repressive H3K27me3 chromatin mark deposited by PRC2. Coupled with our ChIP-qPCR data showing increased H2K27me3 and PRC2 binding at cell cycle genes in BAF53a mutant cells, this suggests that BAF53a regulates cell cycle progression and NSPC maintenance in part by antagonizing PRC2. NSPC proliferation is thus regulated by direct opposition between npBAF complexes and PRC2 at BAF53a target sites. This finding is consistent with previous studies in ES cells and fibroblasts demonstrating that deletion of *Brg1* results in increased H3K27me3 near BRG1 peaks and that recruitment of BAF complexes to repressive chromatin leads to PRC2 eviction and loss of H3K27me3 marks within minutes (Ho et al. 2011; Kadoch et al. 2017; Stanton et al. 2017). The ability of BAF complexes to rapidly and directly evict Polycomb by an ATP-dependent mechanism likely underlies their role in the development of accessibility for pioneer TFs like ASCL1 and SOX2, which play critical roles in cortical development. It was recently shown that disruption of PRC2 in the embryonic cortex, via conditional deletion of core subunit *Eed*, reduces H3K27me3 levels, altering the time course of NSPC differentiation, resulting in precocious generation of later-born upper layer neurons (Telley et al. 2019). In line with these findings, we observe the opposite phenotype in our BAF53a mutants, in which cell cycle progression is blocked and generation of later-born cell types is broadly impaired. In addition to Polycomb-mediated repression, other factors such as DNA methylation levels are known to regulate TF activity (Stadler et al. 2011). In future studies, it would be interesting to determine the role of DNA methylation on BAF53a-dependent chromatin remodeling in the developing brain. The findings presented here highlight a central role for chromatin regulators in the output of NSPCs during brain development. We propose that antagonism between BAF and Polycomb complexes alters the balance of repressive and active chromatin states at specific TF motifs and cell cycle genes to directly regulate cell cycle exit in the developing nervous system.

Materials and methods

Animals

All animal experiments were approved by the Stanford University and University of California at San Francisco Institutional Animal Care and Use Committees and conducted in accordance with National Institutes of Health guidelines for the care and use of laboratory animals. Heterozygous mice carrying a germline deletion were intercrossed to generate *Baf53a*$^{\text{null}}$ mice (*Baf53a*$^{+/-}$). *Baf53a*$^{\text{fl/fl}}$ mice (Krasteva et al. 2012) were mated with *Baf53a*$^{+/-}$; *Nestin-Cre* mice (Imayoshi et al. 2006) to generate conditional knockout pups. Transgenic mice expressing constitutively active β-catenin (Chenn and Walsh 2002) were bred with *Nestin-Cre* mice. All the lines have been backcrossed to C57BL/6J background for a minimum of seven generations. Genotyping was performed by PCR of tail DNA at 3 wk when weaning.

In utero electroporation

Timed pregnant Swiss Webster dams (Charles River) or dams carrying *Baf53a* mutant alleles (*Baf53a*^{fl} or *Baf53a*^{null}) at E13.5 were deeply anesthetized using isofluorane inhalation anesthesia, and the uterine horns were exposed. One microliter (concentration 3 µg/µL) of control plasmid (GFP), or a mix of GFP and a polycistronic nBAF (pCAG-53b-CREST-45b) or npBAF (pCAG-53a-SS18-45d) vector was injected into the lateral ventricles using a sterile glass microinjection pipette. The E13.5 embryos were then electroporated through the uterine wall using square pulse electroporator (BTX 830) with five 50-msec pulses of 38 V. Following electroporation, the uterine horns were placed back into the dam for the embryos to recover and grow. For quit fraction analyses, the pregnant dam was injected intraperitoneally with 50 mg/kg BrdU at E14.5 (24 h postelectroporation), and embryonic brains were harvested 24 h postinjection at E15.5. A minimum of $n = 3$ embryos from at least two different litters were used for each analysis.

Neural stem/progenitor cell cultures

Single cells were dissociated from E12.5 embryonic forebrains and cultured in suspension in DMEM/F-12 (Life Technologies 10565-042) containing N2 supplement (Life Technologies 17502-048), B27 supplement (vitamin A minus, Life Technologies 12587-010), HEPES (Invitrogen 15630080), nonessential amino acids (Invitrogen 11140050), GlutaMAX (Invitrogen 35050061), penicillin/streptomycin (Invitrogen 15140122), and ß-mercaptoethanol (Invitrogen 21985023). bFGF (Invitrogen 13256-029) and EGF (Invitrogen PHG0311) growth factors were used as mitogens to maintain proliferative NSPC cultures. For passaging, the neurospheres were digested with papain

(Worthington LS003126) and mechanically dissociated into single cells. NSPCs were subsequently grown on polyornithine coated dishes for adherence. For the in vitro rescue experiments, adherent cultures of *Actin-CreER;Baf53a*$^{fl/-}$ NSPCs were infected with lentiviruses and selected with puromycin for 3 d followed by 3 d of tamoxifen (TAM) treatment to delete *Baf53a*. Cells were maintained in proliferative conditions by supplementing the culture media with EGF and bFGF growth factors.

Immunohistochemistry

For immunocytochemistry, cells were fixed with 4% PFA for 10 min at 4°C. Antibodies used were NESTIN (DSHB; rat-401), Map2ab (Millipore MAB378Tuj1), BAF53a (Novus NB100-61628), and BAF53b (Crabtree laboratory). Mouse embryonic brain tissue was collected at various time points from electroporated wild-type and BAF53a mutants animals, fixed in ice-cold 4% PFA (EMS 15710) for 30 min on ice (or overnight at 4°C for E18–P0 brains), and cryoprotected in 30% sucrose before embedding in OCT (Sakura 4583) and sectioned on a Leica cryostat at 16 µm. Sections were kept frozen at −80°C until needed for staining. Sections were blocked in 5% serum in 0.25% TritonX/PBS and incubated in primary antibody overnight. Primary antibody binding was detected using Alexa fluorophore-conjugated secondary antibodies (Thermo Fisher Scientific). For BrdU immunostaining, brain sections were first stained for all other antigens and then postfixed in ice-cold 4% PFA before undergoing antigen retrieval (30-min incubation in 2N HCl at 37°C) and then incubated in anti-BrdU primary antibody overnight. Brain sections were incubated for 30 min in 95°C citrate buffer (pH 6) prior to staining for CUX1. Antibodies used for immunofluorescent tissue staining included KI67 (BD Pharmingen 550609), PH3 (Millipore Sigma 160189), BrdU (Abcam ab6326), CC3 (Cell Signaling Technology 9664), GFP (Abcam ab13970), pVIM (Abcam ab22651), SOX2 (Santa Cruz Biotechnology sc17320), Tbr2/Eomes (Thermo Fisher 14-4875-82), DCX (Santa Cruz Biotechnology sc8066), MAP2ab (Millipore Sigma MAB378), NEUN (Millipore Sigma MAB1281), TBR1 (Abcam ab31940), CTIP2 (Abcam ab18465), SATB2 (Abcam ab51502), CUX1 (Santa Cruz Biotechnology sc13024), BRN1 (Novus Biologicals NBP1-49872), SOX9 (R&D Systems AF3075), BLBP (Abcam ab32423), and OLIG2 (Millipore Sigma AB9610).

Microscopy and image analysis

Images were acquired on an upright epifluorescent Zeiss Axioscope Imager.M2 using a 20× objective, as well as a Keyence BZ-X700 microscope, and processed using Adobe Photoshop CC2019. For quantitative analysis, cells within the 20× field view were counted manually using the ImageJ (public domain BSD-2) Cell Counter application. Cell counts were performed on a minimum of three region-matched brain sections per animal and for a minimum of three area-matched regions of interest per coverslip. Results were plotted and analyzed using Prism 8 (GraphPad).

FACS analysis

NSPC cultures were labeled with BrdU (BD Pharmingen 559616) for 1 h or 2 h, respectively. Trypsinized cells were processed for BrdU-FITC and 7AAD (7-aminoactinomycin D) staining following the manufacturer's protocol (BD Pharmigen 559616). FACS was run on a Scanford analyzer (Stanford FACS Core Facility), and data were analyzed using Flowjo software.

Immunoprecipitation

Immunoprecipitations were performed on 250 µg of nuclear extracts prepared as previously described in Kadoch and Crabtree (2013). Immunoprecipitation antibodies (2.5 µg) were incubated with nuclear extracts rotating overnight at 4°C, and then protein G Dynabeads were used to isolate Ig-protein complexes with 2-h incubation rotating at 4°C.

Western blot

The following antibodies were used for the western blots: mouse anti-Brg1 (1:1000; Santa Cruz Biotechnology sc-17796), rabbit anti-Suz12 (1:1000; Cell Signaling 3737), rabbit anti-actin (1:500; Sigma A2066), rabbit anti-H3 (1:2000; Abcam), rabbit anti-BAF53a (1:1000; Novus NB100-61628), rabbit anti-Epc-1 (1:1000; Abcam ab5514), rabbit anti-Tip60 (1:500; Millipore 07-038), and mouse anti-β-actin (1:1000; Abcam ab6276). Antibodies against BAF subunits were generated in our laboratory and used at the following concentrations: BAF53b (1:500), BAF45d (1:2000), and BAF155 (1:1000). The secondary antibodies were goat anti-rabbit or mouse conjugated with IRDye 680RD or 800CW. Images were taken and quantified using an Odyssey/LiCor fluorescence imaging system.

Differential salt extraction of chromatin-associated proteins

Nuclei from NSPCs were isolated using Buffer A (25 mM HEPES at pH 7.6, 5 mM $MgCl_2$, 25 mM KCl, 0.05 mM EDTA, 10% glycerol, 0.1% NP-40) and aliquoted into separate tubes for further treatment. Pellets were resuspended in buffer A with different NaCl concentrations as indicated and were rotated for 30 min at 4°C, followed by high-speed centrifugation for 15 min to pellet insoluble chromatin. Nuclear lysates were removed and mixed with 4× gel loading dye for western blot analysis. The chromatin fraction was solubilized for western blot by sonication.

Anaphase bridge analysis

Analysis was performed as previously described in Dykhuizen et al. (2013). Seventy-two hours after tamoxifen treatment, cells were fixed with 4% paraformaldehyde for 20 min and washed with PBS, and DNA content was visualized by staining with1 µg/mL 49,6-diamidino-2-phenylindole (DAPI; Sigma) to detect and count anaphase bridges.

ATPase assay

Assay was performed as previously described in Dykhuizen et al. (2013). Immunoprecipitates were washed with 10 mM Tris-HCl, (pH 7.5), 50 mM NaCl, 5 mM $MgCl_2$, and 1 mM DTT and resuspended in assay buffer (10 mM Tris-HCl at pH 7.5, 50 mM NaCl, 5 mM $MgCl_2$, 20% glycerol, 1 mg/mL BSA, 0.2 mM ATP, 20 nM plasmid DNA, 50 mCi mL^{-1} γ-^{32}P ATP, 1 mM DTT, protease inhibitors). The reaction was agitated for 1 h at 37°C. Reaction mixtures were spotted onto PEI cellulose plates at the indicated time points, and thin layer chromatography was performed in 0.5 M LiCl and 1 M formic acid. The plates were dried and imaged using phosphorimaging.

Glycerol gradient

The glycerol gradient was prepared in HEMK buffer (25 mM HEPES, 0.1 mM EDTA, 12.5 mM $MgCl_2$, 100 mM KCl) using a Hoefer SG 15 gradient maker (GE Healthcare Bio-Sciences). Three-hundred micrograms of nuclear extract from *Baf53a*$^{f/-}$:

Actin-CreER cells with or without tamoxifen was loaded onto the top of the gradient and separated by ultracentrifugation at 40,000 rpm for 16 h at 4°C. Five-hundred microliters of fractions was collected from top to bottom and precipitated by TCA. Precipitates were washed twice with acetone, air-dried, and resuspended in 1× LDS loading buffer for western blotting.

Plasmid construction and viral preparation

cDNAs of BAF53a, BAF53b, and all other genes used in this study were cloned downstream from the EF1a promoter in a lentiviral construct with puromycin, hygromycin, or blasticidin selection. The *miR-9/-124* lentiviral construct was reported before in Yoo et al. (2011). Lenti-X 293T cells (Clontech 632180) were transfected with appropriate amounts of lentiviral constructs, psPAX2 and pMD2.G, using PEI (Polysciences 24765-2) after reaching 70%–80% confluence. Medium was replaced 16 h after transfection, and virus was harvested after 48 h. Virus was filtered and spun down by ultracentrifuge for enrichment. The pellet was resuspended for infection. For in utero electroporation experiments, polycistronic vectors were cloned to generate pCAG-53b-CREST-45b (nBAF) and pCAG-53a-SS18-45d (npBAF) constructs, which were coelectroporated with reporter pCAG-GFP plasmids.

RNA-seq and data analysis

RNA-seq libraries were prepared as previously described (Sood et al. 2020). In brief, E15.5 forebrains from *Baf53a* Het and cKO mice were dissociated into single cells and total RNA was extracted. The sequencing libraries were made from 1 µg of RNA using the SMARTer kit (Takara Bio) and sequenced on an Illumina Nextseq. RNA-seq reads were processed by mapping to the mm10 reference mouse genome using Kallisto. Differential peak calls were made using DESeq2 (Love et al. 2014) and the requirement was set at fold changes of >1.5-fold in either direction and FDR-corrected $P < 0.10$. DAVID software was used to determine gene ontology (GO) terms for biological functions associated with the up-regulated and down-regulated genes.

ATAC-seq and data analysis

ATAC-seq libraries were prepared as previously described (Sood et al. 2020). In brief, E15.5 forebrains from *Baf53a* Het and cKO mice were dissociated into single cells. Fifty-thousand viable cells per sample was resuspended in 50 µL of transposition mix (Illumina) and incubated for 30 min at 37°C. Libraries were amplified by PCR with barcoded Nextera primers and sequenced on an Illumina Nextseq. ATAC-seq reads were processed by mapping to the mm10 reference mouse genome using Bowtie2, rejecting reads that contained more than a single mismatch. Duplicate reads were discarded, leaving only unique reads. Peak calling was performed by MACS2. Differential peak calls were made using DESeq2 and the requirement was set at fold changes of >1.5-fold in either direction and FDR-corrected $P < 0.10$. RPM values in genome tracks are the mean values across replicates from each condition. Deeptools was used to produce heat maps of mean read density across all peaks. ChromHMM (Ernst and Kellis 2017) was used for feature analysis using an eight-state model based on mouse E15.5 forebrain ChIP-seq data analyzed and obtained from Encode. GREAT software was used to annotate ATAC peaks with genes to determine gene ontology terms associated with changes in accessibility (McLean et al. 2010).

BaGFoot footprint depth and flanking accessibility calculation

We used TF binding motifs from the JASPAR motif database (Fornes et al. 2019), 579 motifs in total. TF footprint depth (FPD) was defined as

$$\mathrm{FPD} = \log_2 \frac{N_{\mathrm{MOTIF}}}{N_{\mathrm{FLANK}}},$$

where N_{MOTIF} is the average number of Tn5 inserts in a [−5 bp, +5 bp] window around the motif center and N_{FLANK} is the average number of Tn5 inserts in the [−55 bp, −6 bp] U [6 bp, 55 bp] window around the motif center, calculated using motifs found in differentially accessed peaks. Flanking accessibility (FA) was defined as

$$\mathrm{FA} = \log_2 \frac{N_{\mathrm{FLANK}}}{N_{BG}},$$

where N_{BG} is the number of Tn5 inserts in the background region defined as an interval [−200 bp, −250 bp] U [200 bp, 250 bp] around the motif center. Only motifs found within ATAC-seq peaks were used in the calculations. To visualize changes in FPD and FA between HET and KO, we used bagplot (Baek et al. 2017).

ChIP-seq analysis

Published ChIP-seq data sets from mouse NPCs for ASCL1, SOX2, OLIG2, and PAX6 (see references in the legend for Fig. 7B) were obtained from the cistrome data browser (data sets passed all quality control standards) (Zheng et al. 2019). Published ChIP-seq data sets from WT mouse forebrains were obtained from Encode (H3K27me3, $n = 2$, E15.5) and the Crabtree laboratory (BRG1, $n = 2$, E10.5). Deeptools was used to produce heat maps of mean read density across down-regulated ATAC-seq peaks.

Homer motif analysis

We performed motif enrichment analysis using HOMER v4.11 (Heinz et al. 2010). We constructed genomic intervals [−250 bp, 250 bp] around summits of peaks exhibiting significant change in accessibility between KO and HET samples. These intervals were used as input for findMotifsGenome.pl that was run with the "-size given" option and other default parameters. We performed motif enrichment analysis for all peaks and separately for peaks exhibiting decreased and increased accessibility in KO relative to WT.

ChIP qPCR

ChIP experiments were performed as previously described in Hathaway et al. (2012). For RT-qPCR, DNA samples were prepared using the SensiFAST SYBR Lo-Rox kit (Bioline, BIO-94020), according to the manufacturer's instructions. Analysis of qPCR samples was performed on a QuantStudio 6 Flex system (Life Technologies).

Statistics

Sample sizes were determined based on previous studies in the field. Statistical analyses were performed using Student's *t*-test for comparisons between two groups, or ANOVA with post-hoc correction for multiple comparisons. All data are presented as mean ± SEM. *P*-values of ≤0.05 were considered statistically significant,

Data availability

RNA-seq and ATAC-seq data sets from *Baf53a* Het and cKO E15.5 forebrains that were generated and analyzed in this study are available in the Gene Expression Omnibus repository (GSE164991). Published sequencing data sets were obtained from the Encode project (reference epigenome in mouse forebrain E15.5) and the Cistrome project (CistromeDB ID: 41849, 55623, 54582, and 55368). Other data and materials are available from the authors upon request.

Competing interest statement

E.J.M. is currently an employee of Verge Genomics, and G.R.C. is a founder and scientific advisor for Foghorn Therapeutics.

Acknowledgments

We thank all members of the Crabtree and Panagiotakos laboratories for helpful discussions, as well as S. Jessberger and K. Majzoub for helpful comments on the manuscript. Microscopy was performed using the Stanford Cell Sciences Imaging Facility. Special thanks to the Villeda laboratory at University of California at San Francisco (UCSF) for sharing their imaging equipment. Next-generation sequencing was performed using the Stanford Functional Genomics Facility. FACS analysis was performed using the Stanford Shared FACS Facility. This work was supported by National Institutes of Health grant NS046789 (to G.R.C.), funding from the Howard Hughes Medical Institute (HHMI; to G.R.C.), and generous support by the UCSF Program for Breakthrough Biomedical Research, Sandler Foundation (to G.P.). G.R.C. is an HHMI Investigator. S.M.G.B. is supported by the Sir James Black GSK fellowship. G.P. is funded by the UCSF Sandler Faculty Fellows Program. The Larry L. Hillblom Foundation provided support to R.P.

Author contributions: G.P. and G.R.C. supervised all aspects of these studies. S.M.G.B., R.P., J.T., G.R.C., and G.P. designed and analyzed the experiments. Experiments were executed by S.M.G.B., R.P., and J.T. with support from A.K., Y.T., and E.L.M. The sequencing data were analyzed by S.M.G.B. and A.K. S.M.G.B., R.P., J.T., G.R.C., and G.P. wrote the paper with help and feedback from the rest of the coauthors.

References

Aizawa H, Hu S-C, Bobb K, Balakrishnan K, Ince G, Gurevich I, Cowan M, Ghosh A. 2004. Dendrite development regulated by CREST, a calcium-regulated transcriptional activator. *Science* **303:** 197–202. doi:10.1126/science.1089845

Baek S, Goldstein I, Hager GL. 2017. Bivariate genomic footprinting detects changes in transcription factor activity. *Cell Rep* **19:** 1710–1722. doi:10.1016/j.celrep.2017.05.003

Barker N, Hurlstone A, Musisi H, Miles A, Bienz M, Clevers H. 2001. The chromatin remodelling factor Brg-1 interacts with β-catenin to promote target gene activation. *EMBO J* **20:** 4935–4943. doi:10.1093/emboj/20.17.4935

Bell S, Rousseau J, Peng H, Aouabed Z, Priam P, Theroux J-F, Jefri M, Tanti A, Wu H, Kolobova I, et al. 2019. Mutations in ACTL6B cause neurodevelopmental deficits and epilepsy and lead to loss of dendrites in human neurons. *Am J Hum Genet* **104:** 815–834. doi:10.1016/j.ajhg.2019.03.022

Bertrand N, Castro DS, Guillemot F. 2002. Proneural genes and the specification of neural cell types. *Nat Rev Neurosci* **3:** 517–530. doi:10.1038/nrn874

Braun S, Kirkland JG, Chory EJ, Husmann D, Calarco JP, Crabtree GR. 2017. Rapid and reversible epigenome editing by endogenous chromatin regulators. *Nat Commun* **8:** 560. doi:10.1038/s41467-017-00644-y

Brocard J, Warot X, Wendling O, Messaddeq N, Vonesch JL, Chambon P, Metzger D. 1997. Spatio-temporally controlled site-specific somatic mutagenesis in the mouse. *Proc Natl Acad Sci* **94:** 14559–14563. doi:10.1073/pnas.94.26.14559

Castro DS, Skowronska-Krawczyk D, Armant O, Donaldson IJ, Parras C, Hunt C, Critchley JA, Nguyen L, Gossler A, Göttgens B, et al. 2006. Proneural bHLH and Brn proteins coregulate a neurogenic program through cooperative binding to a conserved DNA motif. *Dev Cell* **11:** 831–844. doi:10.1016/j.devcel.2006.10.006

Chenn A, Walsh CA. 2002. Regulation of cerebral cortical size by control of cell cycle exit in neural precursors. *Science* **297:** 365–369. doi:10.1126/science.1074192

Coller HA, Grandori C, Tamayo P, Colbert T, Lander ES, Eisenman RN, Golub TR. 2000. Expression analysis with oligonucleotide microarrays reveals that MYC regulates genes involved in growth, cell cycle, signaling, and adhesion. *Proc Natl Acad Sci* **97:** 3260–3265. doi:10.1073/pnas.97.7.3260

The Deciphering Developmental Disorders Study. 2015. Large-scale discovery of novel genetic causes of developmental disorders. *Nature* **519:** 223–228. doi:10.1038/nature14135

Dehay C, Kennedy H. 2007. Cell-cycle control and cortical development. *Nat Rev Neurosci* **8:** 438–450. doi:10.1038/nrn2097

Downes CS, Clarke DJ, Mullinger AM, Giménez-Abián JF, Creighton AM, Johnson RT. 1994. A topoisomerase II-dependent G2 cycle checkpoint in mammalian cells. *Nature* **372:** 467–470. doi:10.1038/372467a0

Dykhuizen EC, Hargreaves DC, Miller EL, Cui K, Korshunov A, Kool M, Pfister S, Cho Y-J, Zhao K, Crabtree GR. 2013. BAF complexes facilitate decatenation of DNA by topoisomerase IIα. *Nature* **497:** 624–627. doi:10.1038/nature12146

Ernst J, Kellis M. 2017. Chromatin-state discovery and genome annotation with ChromHMM. *Nat Protoc* **12:** 2478–2492. doi:10.1038/nprot.2017.124

Eroglu E, Burkard TR, Jiang Y, Saini N, Homem CCF, Reichert H, Knoblich JA. 2014. SWI/SNF complex prevents lineage reversion and induces temporal patterning in neural stem cells. *Cell* **156:** 1259–1273. doi:10.1016/j.cell.2014.01.053

Fornes O, Castro-Mondragon JA, Khan A, van der Lee R, Zhang X, Richmond PA, Modi BP, Correard S, Gheorghe M, Baranašić D, et al. 2019. JASPAR 2020: update of the open-access database of transcription factor binding profiles. *Nucleic Acids Res* **172:** 650–656.

Graham V, Khudyakov J, Ellis P, Pevny L. 2003. SOX2 functions to maintain neural progenitor identity. *Neuron* **39:** 749–765. doi:10.1016/S0896-6273(03)00497-5

Grandori C, Cowley SM, James LP, Eisenman RN. 2000. The Myc/Max/Mad network and the transcriptional control of cell behavior. *Annu Rev Cell Dev Biol* **16:** 653–699. doi:10.1146/annurev.cellbio.16.1.653

Hathaway NA, Bell O, Hodges C, Miller EL, Neel DS, Crabtree GR. 2012. Dynamics and memory of heterochromatin in living cells. *Cell* **149:** 1447–1460. doi:10.1016/j.cell.2012.03.052

Heinz S, Benner C, Spann N, Bertolino E, Lin YC, Laslo P, Cheng JX, Murre C, Singh H, Glass CK. 2010. Simple combinations of lineage-determining transcription factors prime *cis*-regulatory elements required for macrophage and B cell identities. *Mol Cell* **38:** 576–589. doi:10.1016/j.molcel.2010.05.004

Ho L, Crabtree GR. 2010. Chromatin remodelling during development. *Nature* **463:** 474–484. doi:10.1038/nature08911

Ho L, Ronan JL, Wu J, Staahl BT, Chen L, Kuo A, Lessard J, Nesvizhskii AI, Ranish J, Crabtree GR. 2009. An embryonic stem cell chromatin remodeling complex, esBAF, is essential for embryonic stem cell self-renewal and pluripotency. *Proc Natl Acad Sci* **106:** 5181–5186. doi:10.1073/pnas.0812889106

Ho L, Miller EL, Ronan JL, Ho WQ, Jothi R, Crabtree GR. 2011. esBAF facilitates pluripotency by conditioning the genome for LIF/STAT3 signalling and by regulating polycomb function. *Nat Cell Biol* **13:** 903–913. doi:10.1038/ncb2285

Hota SK, Bruneau BG. 2016. ATP-dependent chromatin remodeling during mammalian development. *Development* **143:** 2882–2897. doi:10.1242/dev.128892

Imayoshi I, Ohtsuka T, Metzger D, Chambon P, Kageyama R. 2006. Temporal regulation of Cre recombinase activity in neural stem cells. *Genesis* **44:** 233–238. doi:10.1002/dvg.20212

Kadoch C, Crabtree GR. 2013. Reversible disruption of mSWI/SNF (BAF) complexes by the SS18-SSX oncogenic fusion in synovial sarcoma. *Cell* **153:** 71–85. doi:10.1016/j.cell.2013.02.036

Kadoch C, Williams RT, Calarco JP, Miller EL, Weber CM, Braun S, Pulice JL, Chory EJ, Crabtree GR. 2017. Dynamics of BAF-Polycomb complex opposition on heterochromatin in normal and oncogenic states. *Nat Genet* **49:** 213–222. doi:10.1038/ng.3734

Kamei Y, Inagaki N, Nishizawa M, Tsutsumi O, Taketani Y, Inagaki M. 1998. Visualization of mitotic radial glial lineage cells in the developing rat brain by Cdc2 kinase-phosphorylated vimentin. *Glia* **23:** 191–199. doi:10.1002/(SICI)1098-1136(199807)23:3<191::AID-GLIA2>3.0.CO;2-8

Kerosuo L, Piltti K, Fox H, Angers-Loustau A, Häyry V, Eilers M, Sariola H, Wartiovaara K. 2008. Myc increases self-renewal in neural progenitor cells through Miz-1. *J Cell Sci* **121:** 3941–3950. doi:10.1242/jcs.024802

Klemm SL, Shipony Z, Greenleaf WJ. 2019. Chromatin accessibility and the regulatory epigenome. *Nat Rev Gen* **20:** 207–220. doi:10.1038/s41576-018-0089-8

Knobloch M, Braun S, Zurkirchen L, von Schoultz C, Zamboni N, Araúzo-Bravo MJ, Kovacs WJ, Karalay O, Suter U, Machado RAC, et al. 2013. Metabolic control of adult neural stem cell activity by Fasn-dependent lipogenesis. *Nature* **493:** 226–230. doi:10.1038/nature11689

Krasteva V, Buscarlet M, Diaz-Tellez A, Bernard M-A, Crabtree GR, Lessard JA. 2012. The BAF53a subunit of SWI/SNF-like BAF complexes is essential for hemopoietic stem cell function. *Blood* **120:** 4720–4732. doi:10.1182/blood-2012-04-427047

Kriegstein A, Alvarez-Buylla A. 2009. The glial nature of embryonic and adult neural stem cells. *Annu Rev Neurosci* **32:** 149–184. doi:10.1146/annurev.neuro.051508.135600

Lessard J, Wu JI, Ranish JA, Wan M, Winslow MM, Staahl BT, Wu H, Aebersold R, Graef IA, Crabtree GR. 2007. An essential switch in subunit composition of a chromatin remodeling complex during neural development. *Neuron* **55:** 201–215. doi:10.1016/j.neuron.2007.06.019

Love MI, Huber W, Anders S. 2014. Moderated estimation of fold change and dispersion for RNA-seq data with DESeq2. *Genome Biol* **15:** 550. doi:10.1186/s13059-014-0550-8

Mao Y, Abrieu A, Cleveland DW. 2003. Activating and silencing the mitotic checkpoint through CENP-E-dependent activation/inactivation of BubR1. *Cell* **114:** 87–98. doi:10.1016/S0092-8674(03)00475-6

Martin C-A, Murray JE, Carroll P, Leitch A, Mackenzie KJ, Halachev M, Fetit AE, Keith C, Bicknell LS, Fluteau A, et al. 2016. Mutations in genes encoding condensin complex proteins cause microcephaly through decatenation failure at mitosis. *Genes Dev* **30:** 2158–2172. doi:10.1101/gad.286351.116

McConnell SK, Kaznowski CE. 1991. Cell cycle dependence of laminar determination in developing neocortex. *Science* **254:** 282–285. doi:10.1126/science.1925583

McLean CY, Bristor D, Hiller M, Clarke SL, Schaar BT, Lowe CB, Wenger AM, Bejerano G. 2010. GREAT improves functional interpretation of *cis*-regulatory regions. *Nat Biotechnol* **28:** 495–501. doi:10.1038/nbt.1630

Mistri TK, Devasia AG, Chu LT, Ng WP, Halbritter F, Colby D, Martynoga B, Tomlinson SR, Chambers I, Robson P, et al. 2015. Selective influence of Sox2 on POU transcription factor binding in embryonic and neural stem cells. *EMBO Rep* **16:** 1177–1191. doi:10.15252/embr.201540467

Ninkovic J, Steiner-Mezzadri A, Jawerka M, Akinci U, Masserdotti G, Petricca S, Fischer J, von Holst A, Beckers J, Lie CD, et al. 2013. The BAF complex interacts with Pax6 in adult neural progenitors to establish a neurogenic cross-regulatory transcriptional network. *Cell Stem Cell* **13:** 403–418. doi:10.1016/j.stem.2013.07.002

Nishi Y, Zhang X, Jeong J, Peterson KA, Vedenko A, Bulyk ML, Hide WA, McMahon AP. 2015. A direct fate exclusion mechanism by Sonic hedgehog-regulated transcriptional repressors. *Development* **142:** 3286–3293. doi:10.1242/dev.124636

Oberst P, Fièvre S, Baumann N, Concetti C, Bartolini G, Jabaudon D. 2019. Temporal plasticity of apical progenitors in the developing mouse neocortex. *Nature* **573:** 370–374. doi:10.1038/s41586-019-1515-6

Olave I, Wang W, Xue Y, Kuo A, Crabtree GR. 2002. Identification of a polymorphic, neuron-specific chromatin remodeling complex. *Genes Dev* **16:** 2509–2517. doi:10.1101/gad.992102

Palmer TD, Ray J, Gage FH. 1995. FGF-2-responsive neuronal progenitors reside in proliferative and quiescent regions of the adult rodent brain. *Mol Cell Neurosci* **6:** 474–486. doi:10.1006/mcne.1995.1035

Santen GWE, Aten E, Sun Y, Almomani R, Gilissen C, Nielsen M, Kant SG, Snoeck IN, Peeters EAJ, Hilhorst-Hofstee Y, et al. 2012. Mutations in SWI/SNF chromatin remodeling complex gene *ARID1B* cause Coffin-Siris syndrome. *Nat Genet* **44:** 379–380. doi:10.1038/ng.2217

Santen GWE, Aten E, Vulto-van Silfhout AT, Pottinger C, van Bon BWM, van Minderhout IJHM, Snowdowne R, van der Lans CAC, Boogaard M, Linssen MML, et al. 2013. Coffin-Siris syndrome and the BAF complex: genotype-phenotype study in 63 patients. *Hum Mutat* **34:** 1519–1528. doi:10.1002/humu.22394

Savage JE, Jansen PR, Stringer S, Watanabe K, Bryois J, de Leeuw CA, Nagel M, Awasthi S, Barr PB, Coleman JRI, et al. 2018. Genome-wide association meta-analysis in 269,867 individuals identifies new genetic and functional links to intelligence. *Nat Genet* **50:** 912–919. doi:10.1038/s41588-018-0152-6

Shimizu T, Nakazawa M, Kani S, Bae Y-K, Shimizu T, Kageyama R, Hibi M. 2010. Zinc finger genes Fezf1 and Fezf2 control neuronal differentiation by repressing Hes5 expression in the forebrain. *Development* **137:** 1875–1885. doi:10.1242/dev.047167

Sniekers S, Stringer S, Watanabe K, Jansen PR, Coleman JRI, Krapohl E, Taskesen E, Hammerschlag AR, Okbay A, Zabaneh D, et al. 2017. Genome-wide association meta-analysis of 78,308 individuals identifies new loci and genes influencing human intelligence. *Nat Genet* **49:** 1107–1112. doi:10.1038/ng.3869

Sood S, Weber CM, Hodges HC, Krokhotin A, Shalizi A, Crabtree GR. 2020. CHD8 dosage regulates transcription in pluripotency and early murine neural differentiation. *Proc Natl Acad Sci* **24:** 201921963.

Stadler MB, Murr R, Burger L, Ivánek R, Lienert F, Schöler A, van Nimwegen E, Wirbelauer C, Oakeley EJ, Gaidatzis D, et al. 2011. DNA-binding factors shape the mouse methylome at distal regulatory regions. *Nature* **480:** 490–495. doi:10.1038/nature10716

Stanton BZ, Hodges C, Calarco JP, Braun S, Ku WL, Kadoch C, Zhao K, Crabtree GR. 2017. Smarca4 ATPase mutations disrupt direct eviction of PRC1 from chromatin. *Nat Genet* **49:** 282–288. doi:10.1038/ng.3735

Sun J, Rockowitz S, Xie Q, Ashery-Padan R, Zheng D, Cvekl A. 2015. Identification of in vivo DNA-binding mechanisms of Pax6 and reconstruction of Pax6-dependent gene regulatory networks during forebrain and lens development. *Nucleic Acids Res* **43:** 6827–6846. doi:10.1093/nar/gkv589

Telley L, Agirman G, Prados J, Amberg N, Fièvre S, Oberst P, Bartolini G, Vitali I, Cadilhac C, Hippenmeyer S, et al. 2019. Temporal patterning of apical progenitors and their daughter neurons in the developing neocortex. *Science* **364:** eaav2522. doi:10.1126/science.aav2522

Tsurusaki Y, Okamoto N, Ohashi H, Kosho T, Imai Y, Hibi-Ko Y, Kaname T, Naritomi K, Kawame H, Wakui K, et al. 2012. Mutations affecting components of the SWI/SNF complex cause Coffin-Siris syndrome. *Nat Genet* **44:** 376–378. doi:10.1038/ng.2219

Tsurusaki Y, Koshimizu E, Ohashi H, Phadke S, Kou I, Shiina M, Suzuki T, Okamoto N, Imamura S, Yamashita M, et al. 2014. De novo SOX11 mutations cause Coffin-Siris syndrome. *Nat Commun* **5:** 4011. doi:10.1038/ncomms5011

Tuoc T, Dere E, Radyushkin K, Pham L, Nguyen H, Tonchev AB, Sun G, Ronnenberg A, Shi Y, Staiger JF, et al. 2017. Ablation of BAF170 in developing and postnatal dentate gyrus affects neural stem cell proliferation, differentiation, and learning. *Mol Neurobiol* **54:** 4618–4635. doi:10.1007/s12035-016-9948-5

Van Houdt JKJ, Nowakowska BA, Sousa SB, van Schaik BDC, Seuntjens E, Avonce N, Sifrim A, Abdul-Rahman OA, van den Boogaard M-JH, Bottani A, et al. 2012. Heterozygous missense mutations in SMARCA2 cause Nicolaides-Baraitser syndrome. *Nat Genet* **44:** 445–9–S1.

Vasileiou G, Ekici AB, Uebe S, Zweier C, Hoyer J, Engels H, Behrens J, Reis A, Hadjihannas MV. 2015. Chromatin-remodeling-factor ARID1B represses Wnt/β-catenin signaling. *Am J Hum Genet* **97:** 445–456. doi:10.1016/j.ajhg.2015.08.002

Victor MB, Richner M, Hermanstyne TO, Ransdell JL, Sobieski C, Deng P-Y, Klyachko VA, Nerbonne JM, Yoo AS. 2014. Generation of human striatal neurons by microRNA-dependent direct conversion of fibroblasts. *Neuron* **84:** 311–323. doi:10.1016/j.neuron.2014.10.016

Vierbuchen T, Ostermeier A, Pang ZP, Kokubu Y, Südhof TC, Wernig M. 2010. Direct conversion of fibroblasts to functional neurons by defined factors. *Nature* **463:** 1035–1041. doi:10.1038/nature08797

Vogel-Ciernia A, Matheos DP, Barrett RM, Kramár EA, Azzawi S, Chen Y, Magnan CN, Zeller M, Sylvain A, Haettig J, et al. 2013. The neuron-specific chromatin regulatory subunit BAF53b is necessary for synaptic plasticity and memory. *Nat Neurosci* **16:** 552–561. doi:10.1038/nn.3359

Wang W, Côté J, Xue Y, Zhou S, Khavari PA, Biggar SR, Muchardt C, Kalpana GV, Goff SP, Yaniv M, et al. 1996a. Purification and biochemical heterogeneity of the mammalian SWI-SNF complex. *EMBO J* **15:** 5370–5382. doi:10.1002/j.1460-2075.1996.tb00921.x

Wang W, Xue Y, Zhou S, Kuo A, Cairns BR, Crabtree GR. 1996b. Diversity and specialization of mammalian SWI/SNF complexes. *Genes Dev* **10:** 2117–2130. doi:10.1101/gad.10.17.2117

Wapinski OL, Vierbuchen T, Qu K, Lee QY, Chanda S, Fuentes DR, Giresi PG, Ng YH, Marro S, Neff NF, et al. 2013. Hierarchical mechanisms for direct reprogramming of fibroblasts to neurons. *Cell* **155:** 621–635. doi:10.1016/j.cell.2013.09.028

Wenderski W, Wang L, Krokhotin A, Walsh J, Li H, Shoji H, Ghosh S, Geroge R, Miller E, Elias L, et al. 2020. Loss of the neural-specific BAF subunit ACTL6B relieves repression of early response genes and causes recessive autism. *Proc Nat Acad Sci* 117**:** 10055–10066. doi:10.1073/pnas.1908238117

Wu JI, Lessard J, Olave IA, Qiu Z, Ghosh A, Graef IA, Crabtree GR. 2007. Regulation of dendritic development by neuron-specific chromatin remodeling complexes. *Neuron* **56:** 94–108. doi:10.1016/j.neuron.2007.08.021

Wu JI, Lessard J, Crabtree GR. 2009. Understanding the words of chromatin regulation. *Cell* **136:** 200–206. doi:10.1016/j.cell.2009.01.009

Yoo AS, Staahl BT, Chen L, Crabtree GR. 2009. MicroRNA-mediated switching of chromatin-remodelling complexes in neural development. *Nature* **460:** 642–646. doi:10.1038/nature08139

Yoo AS, Sun AX, Li L, Shcheglovitov A, Portmann T, Li Y, Lee-Messer C, Dolmetsch RE, Tsien RW, Crabtree GR. 2011. MicroRNA-mediated conversion of human fibroblasts to neurons. *Nature* **476:** 228–231. doi:10.1038/nature10323

Zheng R, Wan C, Mei S, Qin Q, Wu Q, Sun H, Chen C-H, Brown M, Zhang X, Meyer CA, et al. 2019. Cistrome Data Browser: expanded datasets and new tools for gene regulatory analysis. *Nucleic Acids Res* **47:** D729–D735. doi:10.1093/nar/gky1094

Zhu B, Ueda A, Song X, Horike S-I, Yokota T, Akagi T. 2017. Baf53a is involved in survival of mouse ES cells, which can be compensated by Baf53b. *Sci Rep* **7:** 14059–14014. doi:10.1038/s41598-017-14362-4